Semiclassical construction of resonances with hyperbolic structure: the scar function

2001 J. Phys. A: Math. Gen. 34 4525

(http://iopscience.iop.org/0305-4470/34/21/308)

INSTITUTE OF PHYSICS PUBLISHING JOURNAL OF PHYSICS A: MATHEMATICAL AND GENERAL

J. Phys. A: Math. Gen. **34** (2001) 4525–4552 www.iop.org/Journals/ja PII: S0305-4470(01)19217-6

Semiclassical construction of resonances with hyperbolic structure: the scar function

Eduardo G Vergini and Gabriel G Carlo

Departamento de Física, Comisión Nacional de Energía Atómica, Av. del Libertador 8250, 1429 Buenos Aires, Argentina

Received 16 November 2000

Abstract

The formalism of resonances in quantum chaos is improved by using conveniently defined creation–annihilation operators. With these operators at hand, we are able to construct transverse excited resonances at a given Bohr-quantized energy. Then, by requiring minimum energy dispersion we obtain solutions in terms of even or odd transverse excitations. These wavefunctions, which are constructed in the vicinity of a periodic orbit with maximum energy localization, provide a precise definition of a *scar function*. These scar functions acquire, in the semiclassical limit, the hyperbolic structure characteristic of unstable periodic orbits.

PACS numbers: 0545M, 0365S, 4505

1. Introduction

A semiclassical theory of short periodic orbits (POs) has recently been developed [1, 2]. This formalism allows us to obtain all the quantum information of a chaotic Hamiltonian system in terms of a very small number (which increases at most linearly with the Heisenberg time) of short POs. This drastic reduction in the number of required POs, with respect to the trace formula [3–5], is possible by the evaluation of interaction between POs.

The first step of the theory is the construction of wavefunctions (highly localized in energy) living in the neighbourhood of a PO. In [1, 2] a construction without transverse excitations is presented; they are the optimal ones in the low-energy region. These wavefunctions, the so-called resonances, are essentially constructed with a transverse Gaussian wavepacket (conveniently selected) evolving along the orbit with a modified transverse motion. This motion, which results after dropping the pure hyperbolic one, describes a bunch of POs surrounding the central orbit. Under this motion, the eigenvectors of the monodromy matrix evolve without the exponential contraction–dilation characteristic of hyperbolic motions, and after one period they return over themselves (up to a minus sign). In the same way, the transverse wavepacket returns over itself differing at most by one phase: the accumulated phase along the orbit. For some energies, the so-called Bohr-quantized energies, this phase

0305-4470/01/214525+28$30.00

is an integral multiple of 2π, and the given functions (being continuous) define the required resonances.

In this paper we are going to show that as the energy increases, it is possible to incorporate transverse excitations into the resonances. The construction of such structures is made simple and systematic by the introduction of creation–annihilation operators acting over the above-mentioned resonances (and for this reason we will also call the resonances without transverse excitations vacuum states). Then, at a given energy, we have a basis of resonances constructed with the same PO. Moreover, the semiclassical Hamiltonian operator acting over such a set acquires a simple expression in terms of the creation–annihilation operators (see equation (36)). With these ingredients at hand, we are able to minimize the energy dispersion explicitly. The solutions obtained in this way bear a close resemblance to previous theoretical and numerical works.

In 1988, Bogomolny [6] represented an averaged squared wavefunction as the sum over a finite number of POs. The contribution of each PO, the so-called scar [7] contribution, although not very amenable to numerical tests, has the essential elements characteristic of hyperbolic structures. In 1989, Berry [8] presented an improved version of Bogomolny's ideas working in phase space; he obtained the spectral Wigner function for each scar contribution. The two authors approximate the motion in the neighbourhood of a PO by a linear map on a transverse Poincaré section. In this respect, on each transverse section to the PO their expressions are approximations (depending on the representation used) to the eigenfunctions of a hyperbolic quadratic Hamiltonian. These eigenfunctions were investigated by Nonnenmacher and Voros [9] in the case of one degree of freedom. We stress that these solutions are not normalizable because the transverse direction has an infinite range. Of course, this is not the case in a bounded system where a finite characteristic length defines its size at a given energy. On the other hand, each PO has a more restrictive length associated with the region where the linear motion works. In any case, for generic unstable POs only a limited transverse region can be considered.

As we mentioned above, a resonance with minimum dispersion is obtained as a sum of resonances with transverse excitations. On each Poincaré section transverse to a PO, this set is restricted to the first excitations (the number depending on the associated transverse region) of a transverse Gaussian wavepacket. When the number of admitted excitations goes to infinity (that is, when the energy goes to infinity or $\hbar$ goes to zero), the dispersion goes to zero. Moreover, the minimum-dispersion resonances (restricted to the section) go to the eigenfunctions of a hyperbolic quadratic Hamiltonian. However, the obtained solutions are normalized and well behaved. For this reason, they are representation independent and although we give them in coordinate representation, it is easy to obtain their Wigner or Husimi representation.

de Polavieja *et al* [10] constructed numerically localized wavefunctions on POs. They are a linear combination of eigenfunctions of the system where the coefficients are their overlaps with a wavepacket located in the vicinity of a point of the PO. Moreover, the coefficients are modulated with a Gaussian function in order to impose low-energy dispersion. These localized structures are very similar to the minimum-dispersion resonances, with even transverse excitations, presented in this paper. Another numerical construction with similar results is presented in [11]. Localized structures on short POs are unveiled by performing successive orthogonal transformations of the eigenfunctions to remove their parametric interaction. Finally, Kaplan and Heller [12] successfully computed localized structures in a modified version of the baker's map. Again, their functions are related to the minimum-dispersion resonances (restricted to a surface of section) with even transverse excitations. Following the above-mentioned references, we will also call the minimum-dispersion resonances constructed in this article *scar functions*. In fact, the constructed wavefunctions provide a clear and precise

definition of a scar function, and this is the required tool for quantifying scarring of individual states.

This paper is organized as follows. Section 2 is devoted to the classical motion in the vicinity of unstable POs. Though only a part of the material of this section is new, the presentation is non-traditional and it is well suited to the semiclassical construction developed in other sections. In section 3 we considerably extend the presentation given in [1] for the construction of resonances without transverse excitations, emphasizing the geometrical interpretation of the construction. The next section contains the construction of resonances with transverse excitations and the evaluation of the semiclassical Hamiltonian operator, in terms of creation–annihilation operators. The explicit form of resonances with minimum energy dispersion is given in section 5. Section 6 is dedicated to the comparison of the obtained semiclassical results with numerical computations. The last section is devoted to final remarks and conclusions.

2. Classical dynamics in the neighbourhood of unstable periodic orbits

In this paper we are going to focus our attention on autonomous Hamiltonian systems with two degrees of freedom. However, the developed ideas can be extended to more degrees in an almost straightforward way. The main purpose of this section is to present the classical elements that we will later need for the semiclassical construction of wavefunctions. In particular, we are going to show that the motion in the neighbourhood of unstable POs can be decomposed into a periodic one and a pure hyperbolic motion; that is, the Floquet theorem.

Let γ be an unstable PO isolated on each energy surface. In other words, the dynamics of the system in the vicinity of the trajectory has hyperbolic structure, the hyperbola branches being defined by the stable and unstable manifold tangential directions (these directions will be called stable and unstable manifolds for simplicity).

In order to apply the semiclassical approximations involved in the present paper we only need two conditions to be satisfied by the classical motion. These are the previously mentioned hyperbolic structure in the neighbourhood of the orbit and that the orbit itself be smooth by pieces in configuration space. Then, we introduce a curvilinear coordinate system choosing the x axis along the trajectory and the y axis perpendicular to it at x. We select $y = 0$ on γ in such a way that x defines the points on the trajectory; that is, $p_x = p_x^\gamma(x)$ and $p_y = p_y^\gamma(x)$ on γ. At a given point on γ, we consider the transverse plane, in phase space, defined by a constant value of x and p_x. Points in this plane will be characterized by a displacement ($\delta y \equiv y$, $\delta p_y \equiv p_y - p_y^\gamma$) of the transverse coordinates with respect to their values on γ. Notice that in general the point (δy, δp_y) does not live in the energy shell defined by γ; the difference is given by $\delta E = -\dot{p}_y\,\delta y$ (because $\dot{y} = 0$ on γ). In particular, $\delta E = 0$ for kinetic plus potential energy Hamiltonians.

The projection of the velocity field for the displacements [13] onto the transverse plane is given by

$$\begin{aligned} \dot{x}(x)\frac{\mathrm{d}\delta y}{\mathrm{d}x}(x) &= \frac{\partial^2 H}{\partial y \partial p_y}(x)\delta y(x) + \frac{\partial^2 H}{\partial {p_y}^2}(x)\delta p_y(x) \\ -\dot{x}(x)\frac{\mathrm{d}\delta p_y}{\mathrm{d}x}(x) &= \frac{\partial^2 H}{\partial y^2}(x)\delta y(x) + \frac{\partial^2 H}{\partial p_y \partial y}(x)\delta p_y(x) \end{aligned} \tag{1}$$

where H is the classical Hamiltonian and $\dot{x}$ is the time variation of x on γ. Of course, this projected velocity field does not give the right evolution. However, the semiclassical construction we are going to describe in the next section only requires the evolution of a

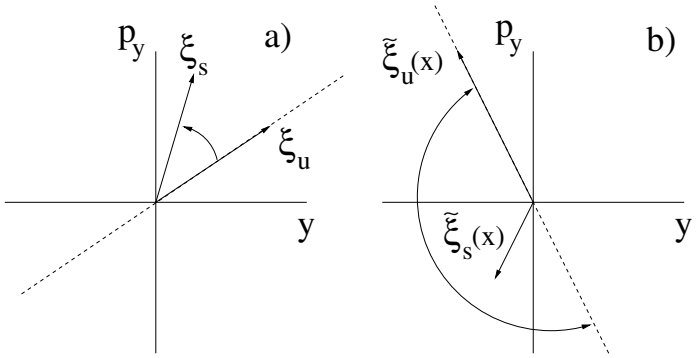

Figure 1. Evolution of the vectors ξ_s and ξ_u, tangential to the stable and unstable manifolds respectively. (*a*) Eigenvectors of the monodromy matrix. (*b*) Evolved eigenvectors at x where the fact that the angle between them is less than π is explicitly noted.

transverse wavepacket for an infinitesimal time. In this respect, the previous equations provide the relevant motion.

As will be discussed later in this section, we need to identify the pure hyperbolic transverse motion. For this reason we are going to work with global solutions of the motion. By integration of the previous equations there results a symplectic matrix $M(x)$ which gives the displacement $(y(x),\ p_y(x))$ (in the following we will eliminate the symbol δ for the displacements in order to simplify the expressions) at x from an initial displacement $(y,\ p_y)$ at $x = 0$

$$\begin{pmatrix} y(x) \\ p_y(x) \end{pmatrix} = \begin{pmatrix} m_{11}(x) & m_{12}(x) \\ m_{21}(x) & m_{22}(x) \end{pmatrix} \begin{pmatrix} y \\ p_y \end{pmatrix}.$$

The evolution along the complete orbit is described by the matrix $M(L)$, L being the length of the orbit. This matrix is the Poincaré return map or transverse monodromy matrix. Its eigenvectors ξ_s and ξ_u define the previously mentioned stable and unstable directions respectively. The eigenvalue corresponding to ξ_u is real with absolute value $\exp(\lambda L)$. The number λ is the orbit's Lyapunov exponent, measured in units of [length^{-1}].

The evolution of ξ_u along the orbit is described by $\tilde{\xi}_u(x) = M(x)\xi_u$. While evolving, this vector dilates and rotates in the y–p_y plane. Let μ be the total number of half turns made by $\tilde{\xi}_u(x)$ during its evolution along the orbit (μ is positive for rotations in the clockwise sense). For even μ, the vector returns to the initial point ($x = L \equiv 0$) on the trajectory with the same direction and sense, and the eigenvalue of ξ_u is positive. For odd μ, its sense changes and the eigenvalue is negative (in this case the motion is called hyperbolic with reflection). We can write

$$\tilde{\xi}_u(L) = (-1)^\mu e^{\lambda L}\xi_u. \tag{2}$$

The vector $\tilde{\xi}_s(x) = M(x)\,\xi_s$ contracts and rotates following $\tilde{\xi}_u(x)$. This rotation is not rigid; the angle between the stable and unstable vectors varies during the evolution. However, this angle is always less than one half turn (see figure 1) because the vectors $\tilde{\xi}_u$ and $\tilde{\xi}_s$ are continuous functions of x and their directions never coincide; that is, the symplectic area $\tilde{\xi}_u(x) \wedge \tilde{\xi}_s(x)$ has a constant non-null value. Then, as the final cumulative rotation of the stable manifold is an integer number of half turns, this number is also μ and we have

$$\tilde{\xi}_s(L) = (-1)^\mu e^{-\lambda L}\xi_s. \tag{3}$$

Since the stable and unstable manifolds rotate during their evolution along the trajectory, it is possible to find values x_0 of x where these directions are symmetrical with respect to

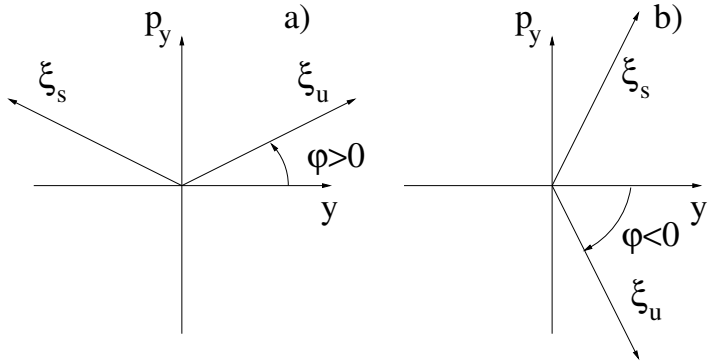

Figure 2. Axes ξ_u and ξ_s on the unstable and stable manifolds respectively, such that their projections on y and p_y are equal in absolute value. (*a*) When the slope of ξ_u is positive. (*b*) When it is negative.

the axes, that is where their slopes in the y–p_y plane are the same in absolute value but with opposite sign. Following the rotations of the manifolds we can find at least 2μ points (exactly 2μ if the swept angles are monotonic functions of x; this is the case for kinetic plus potential energy Hamiltonians [14]) on the orbit satisfying that condition. These points are not canonical invariants as μ or λ are; however, they are invariant under physical unit changes. As a matter of fact, the wave mechanics that we want to describe behaves in the same way.

By finding one of these points we will be able to define the resonances that will be introduced in the next section. Actually, the existence of such points is not essential for the semiclassical construction. However the decomposition of the transverse motion, into a periodic and a hyperbolic one, requires the definition of a function along the orbit (the function $f(x)$ in equation (7)), and the mentioned points provide an efficient tool for such a definition.

The return map M_{x_0} starting at $x = x_0$ (it describes the linear evolution of the transverse coordinates at $x = x_0$, after one period) is related to $M(x)$ as follows:

$$M_{x_0} = M(x_0)M(L)M(x_0)^{-1}. \tag{4}$$

Moreover, the eigenvectors of M_{x_0} acquire the form $(y, p_y) = (a, \pm b)$ with $a, b \neq 0$ (the symmetrical condition) if and only if their diagonal elements are equal. Then, by using this condition and equation (4) it is easy to find x_0. In systems with time reversal, turning points (the orbit being a libration) satisfy such a condition.

We select the origin $x = 0$ at one of these points. With this choice and using the eigenvalues given in equations (2) and (3), the monodromy matrix $M(L)$ acquires the form

$$M(L) = (-1)^{\mu} \begin{pmatrix} \cosh(\lambda L) & \sinh(\lambda L)/\tan(\varphi) \\ \sinh(\lambda L)\tan(\varphi) & \cosh(\lambda L) \end{pmatrix} \tag{5}$$

where $\tan(\varphi)$ in units of [momentum/length] defines the slope of the unstable manifold in the plane y–p_y (where the slope of the stable manifold is $-\tan(\varphi)$). According to the symmetrical condition, the slope is not null.

In general it is impossible to compare vectors living in the plane y–p_y because the axes have different units. However, when the directions are symmetrical with respect to the axes it is only necessary to compare one component. Then, we change to new axes ξ_u and ξ_s on the unstable and stable manifolds respectively, such that their projections on each axis are equal in absolute value. The symplectic matrix B transforming coordinates from the new axes into

the old ones and its inverse are

$$B = (\xi_u \xi_s) = \frac{1}{\sqrt{2}} \begin{pmatrix} 1/\alpha & -s/\alpha \\ s\alpha & \alpha \end{pmatrix} \qquad B^{-1} = \frac{1}{\sqrt{2}} \begin{pmatrix} \alpha & s/\alpha \\ -s\alpha & 1/\alpha \end{pmatrix} \tag{6}$$

with $\alpha = \sqrt{|\tan(\varphi)|}$ and $s = \text{sign}(\varphi)$. We took ξ_u as the first vector of the new basis by convention. Figure 2 shows the two possibilities according to the sign of φ. A straightforward calculation using equations (5) and (6) shows that $B^{-1}M(L)B = (-1)^\mu \exp(\lambda L D)$, with D a diagonal matrix of elements $d_{11} = 1$ and $d_{22} = -1$.

Now, we decompose $M(x)$ into a periodic matrix $F(x)$ describing the evolution of the manifolds, and a matrix (depending in a simple way on x) describing the exponential contraction–dilation along the manifolds,

$$M(x) = F(x) \exp[f(x)\lambda K] \tag{7}$$

where

$$K \equiv BDB^{-1} = \begin{pmatrix} 0 & 1/\tan(\varphi) \\ \tan(\varphi) & 0 \end{pmatrix}$$

verifies $K\xi_u = \xi_u$ and $K\xi_s = -\xi_s$. $f(x)$ is a real function satisfying $f(0) = 0$ and $f(L) = L$.

Equation (7) defines $F(x)$ in terms of $M(x)$

$$F(x) \equiv M(x) \exp[-f(x)\lambda K] \tag{8}$$

and we can see from equation (8) that $F(L) = (-1)^\mu 1$ by evaluating its action on ξ_u and ξ_s. The function $f(x)$ establishes the relation between the lengths of $\tilde{\xi}_u(x)$ and ξ_u whenever possible. However, the lack of a norm in the plane y–p_y makes this task in general impossible. In [1] the function $f(x) = x$ was considered for simplicity; it gives a uniform increment of the length with x; another possible function is $f(x) = t(x)L/T$ (with T the period of γ) giving a uniform increment with time (see section 7 for a further discussion about $f(x)$). We emphasize that the decomposition given in equation (7) represents the Floquet theorem [15], which can also be applied to systems with many transverse directions.

From now on, we consider the matrix $F(x)$ by its action on ξ_u and ξ_s; that is, we define the periodic functions $y_u(x)$, $p_u(x)$, $y_s(x)$ and $p_s(x)$ as follows:

$$\begin{pmatrix} y_u(x) \\ p_u(x) \end{pmatrix} \equiv \xi_u(x) \equiv F(x)\xi_u = \mathrm{e}^{-f(x)\lambda} M(x)\xi_u \tag{9}$$

and

$$\begin{pmatrix} y_s(x) \\ p_s(x) \end{pmatrix} \equiv \xi_s(x) \equiv F(x)\xi_s = \mathrm{e}^{f(x)\lambda} M(x)\xi_s. \tag{10}$$

Equations (9) and (10) shows that it is not necessary to evaluate explicitly $F(x)$. On the other hand, the area preserving property of $F(x)$ guarantees the following condition:

$$y_u(x)p_s(x) - y_s(x)p_u(x) = \xi_u(x) \wedge \xi_s(x) = \xi_u \wedge \xi_s = J \tag{11}$$

where J is the selected unit area in the y–p_y plane (e.g. $J = 1$ Joule-seg.).

The motion described by the modified symplectic matrix $F(x)$ is very unusual: it is neither hyperbolic nor elliptic. It is a neutral motion where all the orbits in the neighbourhood of the central one are also periodic with period L, or $2L$ if μ is an odd number.

In order to know the error introduced by the modified motion we evaluate the action of the right classical transverse evolution, for infinitesimal times, on the vectors $\xi_u(x)$ and $\xi_s(x)$. The evolution from x to $x + \delta x$ is given by $M_x(\delta x) = M(x + \delta x)\, M(x)^{-1}$. So, using equation (8) and that $f(x + \delta x) \simeq f(x) + \delta x f'(x)$, it transpires that

$$M_x(\delta x)F(x) \simeq F(x + \delta x) \exp[\delta x f'(x)\lambda K]$$

where the prime denotes differentiation with respect to x. Then, using (9) or (10) we have to first order in δx

$$\begin{aligned} M_x(\delta x)\xi_{\rm u}(x) &\simeq [1+\delta x f'(x)\lambda]\xi_{\rm u}(x+\delta x) \\ M_x(\delta x)\xi_{\rm s}(x) &\simeq [1-\delta x f'(x)\lambda]\xi_{\rm s}(x+\delta x). \end{aligned} \tag{12}$$

The above expressions show clearly the approximation involved in the construction. We have forced the vector $\xi_{\rm u}$ ($\xi_{\rm s}$) to evolve without dilation (contraction) whilst the right evolution dilates (contracts) the vector at a rate specified by λ.

The classical expressions obtained up to here are enough for the semiclassical construction developed in the following sections. However, in order to give a local motion point of view and to provide an alternative way of deriving the semiclassical expressions, we are going to evaluate the quadratic transverse Hamiltonians $H_{\rm p}$ and $H_{\rm h}$ associated with the periodic and to the pure hyperbolic motion respectively.

$H_{\rm p}$ must provide the velocity field defined by the periodic functions; for instance

$$\dot{y}_{\rm u}(x) = \dot{x}(x)y'_{\rm u}(x).$$

On the other hand, $H_{\rm h}$ must provide the velocity field obtained from equations (12)

$$\dot{\xi}_{\rm u}(x) = \lambda\dot{x}(x)f'(x)\xi_{\rm u}(x) \qquad \text{and} \qquad \dot{\xi}_{\rm s}(x) = -\lambda\dot{x}(x)f'(x)\xi_{\rm s}(x).$$

Then, by requiring the previous relations to be satisfied by Hamilton's equations and using (11), we arrive at the following expressions for $H_{\rm p}$ and $H_{\rm h}$ (for simplicity the arguments are not shown):

$$H_{\rm p} = \frac{\dot{x}}{2J}\big[(y_{\rm u}y'_{\rm s} - y_{\rm s}y'_{\rm u})p_y^2 + 2(p_{\rm s}y'_{\rm u} - p_{\rm u}y'_{\rm s})yp_y + (p_{\rm u}p'_{\rm s} - p_{\rm s}p'_{\rm u})y^2\big] \tag{13}$$

and

$$H_{\rm h} = \frac{\lambda\dot{x}f'}{J}\big[-y_{\rm u}y_{\rm s}p_y^2 + (y_{\rm u}p_{\rm s} + p_{\rm u}y_{\rm s})yp_y - p_{\rm u}p_{\rm s}y^2\big]. \tag{14}$$

In conclusion, we have considered a synchronized motion approximation where all the orbits in the vicinity of the central one move with the same value of x and p_x. Moreover, by virtue of Floquet's theorem we have decomposed the transverse motion into one of periodic nature and another of hyperbolic character. In this approximation, the Hamiltonian takes the form

$$H(x,\,p_x,\,y,\,p_y) \simeq H_{\parallel}(x,\,p_x) + H_{\rm p}(y,\,p_y,\,x) + H_{\rm h}(y,\,p_y,\,x) \tag{15}$$

with $H_{\parallel}(x,\,p_x) \equiv H(x,\,p_x,\,0,\,p_y^{\gamma}(x))$. Observe that $\partial H_{\parallel}/\partial x = \partial H/\partial x$ on γ because $\partial H/\partial p_y = \dot{y} = 0$ on γ; that is, the previous definition does not change the velocity field along the orbit.

The variable x appearing in $H_{\rm p}$ and $H_{\rm h}$ plays the role of the time. So, we have an autonomous one-dimensional Hamiltonian along the orbit and two transverse Hamiltonians depending periodically on the time. In the following sections we will construct semiclassically a basis of eigenfunctions for the restricted Hamiltonian $H_{\parallel} + H_{\rm p}$. Later we will minimize the dispersion introduced by $H_{\rm h}$ in that basis.

3. Resonances of periodic orbits. The vacuum state

In this section we are going to construct a family of wavefunctions associated with a given PO γ. The members of this family are labelled with the number n of excitations along the orbit, and this number defines the energy of the orbit through the Bohr–Sommerfeld quantization rule.

The construction depends only on the motion in the neighbourhood of the orbit; then, it can be applied to bound or open systems in the same way. Following [1] we call these wavefunctions resonances. However, in the next section we will show that each one of them defines a vacuum state over which a finite number of transverse excited states can be created. So, a resonance of γ will be identified with two numbers (n and m) representing the excitations along and transverse to the orbit respectively. For this reason, we will also call the resonances obtained in this section (where $m = 0$) vacuum states.

In the previous section we have shown that the transverse motion can be decomposed into a periodic one defined globally by $F(x)$ and locally by $H_{\mathrm{p}}(y, p_y, x)$, and a pure hyperbolic motion defined by $\exp[f(x)\lambda K]$ or $H_{\mathrm{h}}(y, p_y, x)$ respectively. For the present construction we will drop the pure hyperbolic motion. Then, we propose as a general recipe for the construction of eigenfunctions of the resulting motion a product of two functions. One function only depends on x and it is the semiclassical approximation for the one-dimensional motion along the orbit. The order $\hbar^{-1}$ is the local plane-wave approximation $\exp(\mathrm{i}S(x)/\hbar)$, with $S(x) = \int_0^x p_x \,\mathrm{d}x$ the action. The following order in $\hbar$ modifies the amplitude of the wave. The square modulus of the amplitude at x is proportional to the classical probability of finding the system there. So, we can write the order $\hbar^0$ as

$$\varphi(x) = \mathrm{e}^{\mathrm{i}S(x)/\hbar}/\sqrt{\dot{x}}. \tag{16}$$

We emphasize that the previous solution is valid for a general one-dimensional Hamiltonian, while the most commonly used expression $\mathrm{e}^{\mathrm{i}S(x)/\hbar}/\sqrt{p_x}$ is only applicable to Hamiltonians of the form kinetic plus potential energy ($p_x^2/2m + V(x)$).

The other required function is

$$\tilde{\phi}(x, y) = \exp[\mathrm{i}(y^2/2\hbar)P(x)/Q(x)]/\sqrt{Q(x)} \tag{17}$$

where $Q(x)$ and $P(x)$ are the coordinates of a complex vector constructed with the manifolds

$$\begin{pmatrix} Q(x) = y_{\mathrm{u}}(x) + \mathrm{i}y_{\mathrm{s}}(x) \\ P(x) = p_{\mathrm{u}}(x) + \mathrm{i}p_{\mathrm{s}}(x) \end{pmatrix} \equiv \xi_{\mathrm{u}}(x) + \mathrm{i}\xi_{\mathrm{s}}(x) = M(x)B \begin{pmatrix} \mathrm{e}^{-f(x)\lambda} \\ \mathrm{i}\mathrm{e}^{f(x)\lambda} \end{pmatrix}. \tag{18}$$

The last relation in equation (18) is obtained from (9) and (10). By virtue of equation (11), the following normalization condition results for the complex vector:

$$Q(x)^* P(x) - Q(x)P(x)^* = 2\mathrm{i}\xi_{\mathrm{u}}(x) \wedge \xi_{\mathrm{s}}(x) = 2\mathrm{i}J. \tag{19}$$

Then, $|Q(x)| > 0$ and $\mathrm{Im}\,[P(x)/Q(x)] = J/|Q(x)|^2 > 0$. Thus, for a fixed value of x, $\tilde{\phi}(x, y)$ describes a Gaussian wavepacket with centre at $y = 0$ and momentum $p_y = 0$, the range of the variable y being order $\sqrt{\hbar}$. Its Wigner distribution is also a Gaussian function [13]

$$W_{\tilde{\phi}}(x, y, p_y) = 2\sqrt{\frac{\pi\hbar}{J}} \exp\left[-\frac{y^2 J}{|Q|^2\hbar} - \frac{(p_y - \alpha y)^2|Q|^2}{J\hbar}\right]$$

with $\alpha = (Q^*P + QP^*)/2|Q|^2$. Using equation (11) it is easy to verify for instance that

$$W_{\tilde{\phi}}[x, y_{\mathrm{u}}(x), p_{\mathrm{u}}(x)] = 2\sqrt{\pi\hbar/J}\mathrm{e}^{-J/\hbar}$$

and in general it is possible to show that $W_{\tilde{\phi}}$ is a constant of the motion given by $F(x)$. Figure 3(a) shows a level curve of $W_{\tilde{\phi}}$ at $x = x_1$, and figure 3(b) shows its new position $x = x_2$ after the evolution. The evolved curve is also a level curve at x_2 with the same value of $W_{\tilde{\phi}}$.

This picture suggests that $\tilde{\phi}(x, y)$ describes the evolution of the transverse wavepacket governed by $F(x)$; in fact, using the expressions obtained from wavepacket propagation [13,16] it is easy to verify this point.

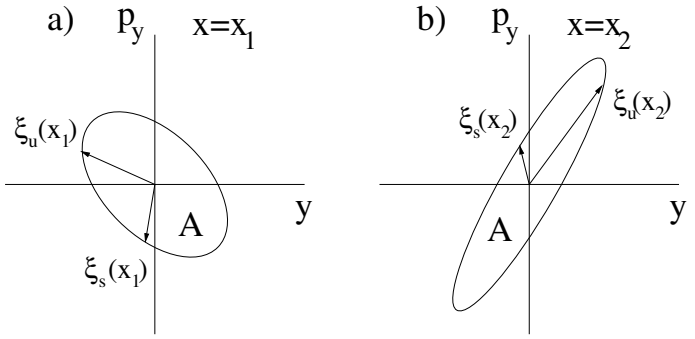

Figure 3. Level curve with enclosed area A of the Wigner representation $W_{\tilde{\phi}}$ of the resonance. The ellipse defined by the vectors of the stable and unstable manifolds rotates and changes its form but preserves this area and corresponds to the same value of $W_{\tilde{\phi}}$. (*a*) Representation at a point x_1 on the trajectory. (*b*) Same as before but after the evolution to x_2.

Another verification of the accuracy of the proposed solution is obtained directly by applying the quantum Hamiltonian to it. A straightforward calculation shows that

$$(\hat{H}_{\parallel} + \hat{H}_{\mathrm{p}} - E)\varphi(x)\tilde{\phi}(x, y) = \mathcal{O}(\hbar^2) \tag{20}$$

where E is the energy of the orbit and $\hat{H}_{\mathrm{p}}$ is the symmetrical quantization ($yp_y \to (\hat{y}\hat{p}_y + \hat{p}_y\hat{y})/2$) of H_{p} (see (13)). To eliminate the order $\hbar^2$ in equation (20) it is necessary to include terms of order $\hbar$ in the solution. However, this is not the right error order of the solution because the considered Hamiltonian is an approximation which does not include terms mixing the variables x and p_x with the transverse ones (see section 2). We show in appendix A, for a Hamiltonian of the form kinetic plus potential energy, that the error of the solution is of order $\sqrt{\hbar}$.

The norm of the proposed solution can be obtained to the leading order in $\hbar$ by integrating the transverse coordinate y (a Gaussian integral), and then the x coordinate. On the other hand, from now on the phase of $Q(x)$ will be a very important ingredient in the semiclassical relations. For these reasons, we are going to use the following normalized expression for the vacuum state:

$$\psi_{\gamma}^{(0)}(x, y) = \frac{\exp\{\mathrm{i}[S(x) + y^2\Gamma(x)/2]/\hbar - \mathrm{i}\phi(x)/2\}}{\sqrt{T\dot{x}}[\pi(\hbar/J)|Q(x)|^2]^{1/4}} \tag{21}$$

with $\Gamma(x) \equiv P(x)/Q(x)$ and T the period of γ. The superscript indicates the number of transverse excitations; in this case it is $m = 0$. $\phi(x)$ is the angle swept by the complex number $Q(x)$ while evolving from 0 to x (the angle is positive in the anticlockwise sense, as usual). It is simple to verify that the total angle $\phi(L)$ swept by $Q(x)$ is equal to the total angle $\pi\mu$ swept by the manifolds (remember that the angle swept by the manifolds is positive in the clockwise sense as defined in section 2). Figure 4(*a*) shows the initial position of the manifolds at $x = 0$. The angle φ is the one defined in equation (5) and we consider the case where $\varphi > 0$; the other case ($\varphi < 0$) can be treated in the same way. Observe that $y_{\mathrm{u}}(0) = -y_{\mathrm{s}}(0) > 0$. Now the manifolds evolve up to the point $x = x_1$ where $y_{\mathrm{u}}(x_1) = y_{\mathrm{s}}(x_1) > 0$ (see figure 4(*b*)). Later, they evolve up to $x = x_2$ where $-y_{\mathrm{u}}(x_2) = y_{\mathrm{s}}(x_2) > 0$ (see figure 4(*c*)), and so on up to $x_N \leqslant L$. Figure 4(*d*) shows the corresponding evolution of Q in the complex plane. The angle ϕ increases by $\pi/2$ each time the system evolves from x_i to x_{i+1}. Taking into account that $\xi_{\mathrm{u}}(L) = (-1)^{\mu}\xi_{\mathrm{u}}$ and $\xi_{\mathrm{s}}(L) = (-1)^{\mu}\xi_{\mathrm{s}}$, because the evolution is determined by $F(x)$, it results that $x_N = L$ with $N = 2\mu$.

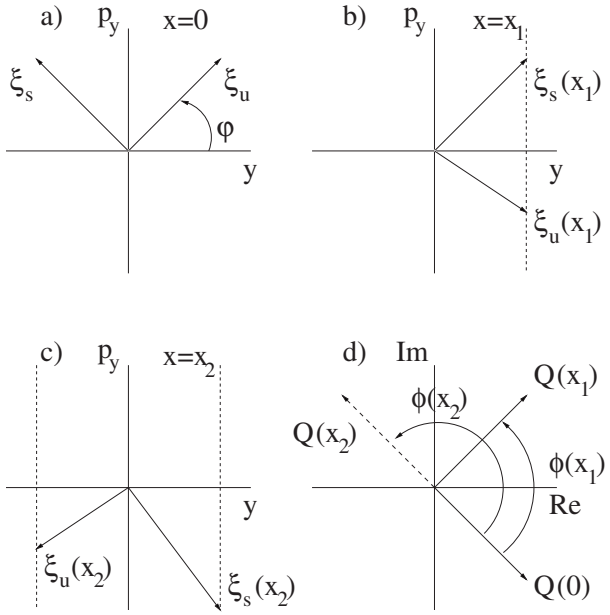

Figure 4. Comparison between the evolution of the complex number $Q(x)$ and the rotation of the manifolds. (*a*) Symmetric initial position of the manifolds. (*b*) The manifolds evolve to x_1. (*c*) Now to x_2. (*d*) Here it is shown how this evolution translates into changes of the number $Q(x)$.

The wavefunction $\psi_\gamma^{(0)}(x, y)$ will be continuous at $x = L$ if the accumulated phase around the orbit $(S(L)/\hbar - \phi(L)/2)$ is an integral multiple of 2π. This condition determines the admitted energies E_γ of the PO and corresponds to the Bohr–Sommerfeld quantization rule:

$$S(L)/\hbar - \mu\pi/2 = 2\pi n \tag{22}$$

where $n = 0, 1, \ldots$ is the number of excitations along γ. Equation (22) predicts the well known phase loss of $\pi/2$ after a smooth potential turning point because in such a case μ increases by one [18]. Moreover, Creagh *et al* [19] have shown that μ is equal to the Maslov index appearing in the trace formula. Actually, this assertion and equation (22) are valid for smooth potentials. However, in hard-wall potentials it is necessary to add a pure quantum phase associated with the boundary conditions; this phase does not have a geometrical interpretation because the classical motion does not take into account whether the wave satisfies Dirichlet or Neumann boundary conditions.

There is a phase loss of π due to Dirichlet boundary conditions while for Neumann conditions the phase does not change. On the other hand, equation (22) predicts a phase loss of $\pi/2$ because μ increases by one after a reflection in a hard-wall potential. Then, in order to give the right changes of phase it is necessary to subtract $\pi/2$ for Dirichlet and to add $\pi/2$ for Neumann. In conclusion, to take into account the boundary conditions in hard-wall potentials, we can rewrite equation (22) as follows:

$$S(L)/\hbar - N_b\pi/2 - \mu\pi/2 = 2\pi n \tag{23}$$

where N_b is the number of reflections satisfying Dirichlet boundary conditions minus the number of reflections satisfying Neumann conditions. Perhaps the decomposition given in

equation (23) (for the change of phase in hard-wall potentials) looks unnecessary. However, we will show in the next section that it is very convenient when the evolution of excitations of transverse wavepackets is considered. With this decomposition, the total accumulated phase given on the left-hand side of equation (23) consists of three contributions: the dynamical phase, a pure quantum phase introduced by boundary conditions and the topological phase associated with the rotations of the manifolds.

For kinetic plus potential Hamiltonians, μ is equal to the number of times the unstable (or stable) manifold becomes parallel to the momentum axis p_y (which is equal to the maximum number of conjugated points), plus the number of turning points in smooth potentials, plus the number of reflections in hard-wall potentials. The manifolds evolve in a continuous way, but at turning points or reflections they change their sense.

Finally, we stress that the semiclassical construction of eigenfunctions in the neighbourhood of *stable* orbits is similar to (21). In this case the initial complex vector $\xi_u + i\xi_s$ of equation (18) is replaced by the eigenvector of the monodromy matrix (a complex vector for stable orbits) satisfying (19). And of course, the evolution of the vector is given by the transverse symplectic matrix without modifications. Eigenvalues have an error $\mathcal{O}(\hbar)$ and eigenfunctions an error $\mathcal{O}(\sqrt{\hbar})$. Moreover, it is possible to improve the accuracy by including transverse excitations [17].

4. Creation–annihilation operators and the pure hyperbolic Hamiltonian

In the previous section we constructed resonances of POs with n excitations along the orbit but without excitations in the transverse direction; we called them vacuum states. In this section we are going to construct resonances with transverse excitations. We will be able to do so by the definition of suitable creation–annihilation operators acting over the vacuum state. Later, we will show that the semiclassical Hamiltonian, when applied to the constructed resonances, can be expressed simply in terms of these operators (see equation (36)).

We begin by demanding that the operators satisfy the usual properties

$$\Lambda \psi_\gamma^{(0)} = 0 \qquad \text{and} \qquad [\Lambda, \Lambda^\dagger] = 1. \tag{24}$$

The general form of Λ (at each value of x) is a linear combination of the transverse operators $\hat{y}$ and $\hat{p}_y$ with the coefficients being complex functions of x; that is, $\Lambda = \alpha(x)\hat{y} - \beta(x)\hat{p}_y$ [17]. Then, by replacing this expression in (24) and using equation (21), we obtain

$$\begin{aligned} &\alpha(x) - \beta(x)P(x)/Q(x) = 0 \\ &\alpha(x)^*\beta(x) - \alpha(x)\beta(x)^* = -\mathrm{i}/\hbar. \end{aligned} \tag{25}$$

Relations (25) plus equation (19) define $\alpha(x)$ and $\beta(x)$ up to a global phase (it is not a function of x).

It is easy to verify that $\psi_\gamma^{(0)}(x = 0, y)$ (see equation (21)) is a real function of y. This selection is very convenient for the construction of real resonances in systems with time reversal invariance. Following the same convention, we select the phase of the creation operator in such a way that $\psi_\gamma^{(m)}(x = 0, y)$ is also real. Then, we obtain the following expressions for the creation–annihilation operators:

$$\begin{aligned} \Lambda &= \mathrm{e}^{-\mathrm{i}\eta}\left(-\mathrm{i}/\sqrt{2J\hbar}\right)[P(x)\hat{y} - Q(x)\hat{p}_y] \\ \Lambda^\dagger &= \mathrm{e}^{\mathrm{i}\eta}\left(\mathrm{i}/\sqrt{2J\hbar}\right)[P(x)^*\hat{y} - Q(x)^*\hat{p}_y] \end{aligned} \tag{26}$$

where η is the phase of $Q(x = 0)$. According to section 2 $\eta = -s\pi/4$, with $s = \mathrm{sign}(\varphi)$ (see figure 2).

Using these operators, a resonance with m transverse excitations is obtained by m applications of $\Lambda^\dagger$ onto the vacuum state

$$\psi_\gamma^{(m)}(x, y) \equiv \Lambda^{\dagger m}\psi_\gamma^{(0)}(x, y)/\sqrt{m!}. \tag{27}$$

With this definition, $\psi_\gamma^{(m)}$ is normalized to unity like $\psi_\gamma^{(0)}$. Moreover, it is possible to prove by induction (see appendix B) that

$$\psi_\gamma^{(m)}(x, y) = \frac{\mathrm{e}^{-\mathrm{i}m\phi(x)}}{\sqrt{2^m m!}} H_m\left[\frac{y\sqrt{J/\hbar}}{|Q(x)|}\right]\psi_\gamma^{(0)}(x, y) \tag{28}$$

where $\phi(x)$ is the phase introduced in equation (21). $H_m(z)$ are the so-called Hermite polynomials; these are polynomials of mth degree in z, defined by the formula $H_m(z) = (-1)^m \mathrm{e}^{z^2} d^m(\mathrm{e}^{-z^2})/\mathrm{d}z^m$ [20]. It is easy to see that $\psi_\gamma^{(m)}$ is also a product of two functions: the solution for the motion along the orbit (see equation (16)) and m excitations of a transverse Gaussian wavepacket which evolves following the periodic motion described by $F(x)$ or $H_\mathrm{p}(y, p_y, x)$.

From equation (28), the accumulated phase of $\psi_\gamma^{(m)}$ around the orbit adds, with respect to $\psi_\gamma^{(0)}$ (see equation (23)), the contribution $-m\phi(L) = -m\pi\mu$ (see section 3) associated with transverse excitations. Then, the generalized Bohr–Sommerfeld quantization rule, guaranteeing the continuity of $\psi_\gamma^{(m)}$ at $x = L \equiv 0$, turns out to be

$$S(L)/\hbar - N_\mathrm{b}\pi/2 - (m + 1/2)\mu\pi = 2\pi n. \tag{29}$$

For even $m\mu$ we can rewrite equation (29) as

$$S(L)/\hbar - N_\mathrm{b}\pi/2 - \mu\pi/2 = 2\pi(n + m\mu/2) \tag{30}$$

and for odd $m\mu$ we can rewrite equation (29) as

$$S(L)/\hbar - N_\mathrm{b}\pi/2 - 3\mu\pi/2 = 2\pi[n + (m - 1)\mu/2]. \tag{31}$$

In this way, the right-hand sides of equations (30) and (31) are given by 2π times an integer number n_0, with $n_0 = 1, 2, \ldots$.

For even μ ($m\mu$ always is even), resonances satisfying $n + m\mu/2 = n_0$ have the same Bohr-quantized energy obtained from equation (30). This set is restricted by two conditions. The first one is $m \geqslant 0$ according to equation (24). The second condition is associated with the limited transverse area A_lin where the linearized motion works; that is, $m < A_\mathrm{lin}/2\pi\hbar$. In order to give a value for A_lin, it is necessary to know the nonlinear motion in the vicinity of the orbit (see section 7). However, for the shortest POs of the system investigated in section 6.1, the criterion $m < n$ (in place of the second one) turns out to be satisfactory.

For odd μ, resonances with odd m quantize at the anti-Bohr energy of the even case. That is, even values of m are treated as stated above (because $m\mu$ is even). On the other hand, odd m resonances satisfying $n + (m - 1)\mu/2 = n_0$ have the Bohr-quantized energy obtained from equation (31) (its value differs from the even case). Moreover, this set is limited by $1 \leqslant m < n$.

In the following we are going to evaluate the application of the semiclassical Hamiltonian operator to resonances. First of all, we will show that resonances with transverse excitations are also eigenfunctions of the restricted Hamiltonian; that is,

$$(\hat{H}_\parallel + \hat{H}_\mathrm{p})\psi_\gamma^{(m)}(x, y) = E_\gamma \psi_\gamma^{(m)}(x, y) + \mathcal{O}(\hbar^2). \tag{32}$$

Taking into account that equation (32) is valid for $m = 0$, we only need to prove that $\hat{H}_\parallel + \hat{H}_\mathrm{p}$ commutes with $\Lambda^\dagger$, but using equations (11), (13) and (26), it is easy to verify that

$$[\hat{H}_\mathrm{p}, \Lambda^\dagger] = -\mathrm{i}\mathrm{e}^{\mathrm{i}\eta}\hbar\dot{x}\,\mathrm{d}\Lambda^\dagger/\mathrm{d}x$$

and

$$[\hat{H}_{\|}, \Lambda^{\dagger}]\varphi(x) = (\mathrm{i}\mathrm{e}^{\mathrm{i}\eta}\hbar\dot{x}\,\mathrm{d}\Lambda^{\dagger}/\mathrm{d}x + \mathcal{O}(\hbar^2))\varphi(x)$$

where $\varphi(x)$ is the solution along the orbit (see equation (16)). Now, using equations (15) and (32), it turns out that

$$(\hat{H} - E_\gamma)\psi_\gamma^{(m)}(x, y) = \hat{H}_{\mathrm{h}}\psi_\gamma^{(m)}(x, y) + \mathcal{O}(\hbar^{3/2}) \tag{33}$$

where $\hat{H}_{\mathrm{h}}$ is the symmetrical quantization of H_{h} (see equation (14)). The order $\hbar^2$ of equation (32) is reduced to $\hbar^{3/2}$ in equation (33) because $H_{\|} + H_{\mathrm{p}} + H_{\mathrm{h}}$ is a synchronized motion approximation of H (see appendix A).

Reference [1] presented another procedure to obtain the application of the semiclassical Hamiltonian to the resonances. Starting with the relations in equation (12), the right evolution transforms the functions $Q(x)$ and $P(x)$ (which were obtained with the modified evolution $F(x)$) into

$$\tilde{Q}(x) = Q(x) + \delta x f'(x)\lambda Q(x)^*$$
$$\tilde{P}(x) = P(x) + \delta x f'(x)\lambda P(x)^*.$$

Then, the application of the semiclassical evolution operator over the resonances gives

$$\hat{U}(\delta t = \delta x/\dot{x})\psi_\gamma^{(m)}(x, y) = \mathrm{e}^{-\mathrm{i}E_\gamma\delta t/\hbar}\tilde{\psi}_\gamma^{(m)}(x, y) \tag{34}$$

where $\tilde{\psi}_\gamma^{(m)}(x, y)$ has the same expression as given in (28) but using the transformed functions $\tilde{Q}(x)$ and $\tilde{P}(x)$. Replacing equation (34) in

$$\hat{H} \equiv \mathrm{i}\hbar \lim_{\delta t\to 0}[\hat{U}(\delta t) - \hat{1}]/\delta t$$

there results after a straightforward but tedious calculation

$$(\hat{H} - E_\gamma)\psi_\gamma^{(m)} = -(s\hbar\dot{x} f'\lambda/2)\left[\sqrt{(m+1)(m+2)}\psi_\gamma^{(m+2)} + \sqrt{(m-1)m}\psi_\gamma^{(m-2)}\right]. \tag{35}$$

We will not give here the direct demonstration (by induction) of equation (35). Nevertheless, we will show that equations (35) and (33) are exactly the same. First of all, by using the definition of $\psi_\gamma^{(m)}$ (see equation (27)) we obtain from equation (35)

$$\hat{H} - E_\gamma = -\frac{s\hbar\dot{x} f'\lambda}{2}(\Lambda^{\dagger 2} + \Lambda^2). \tag{36}$$

Then by writing Λ and $\Lambda^{\dagger}$ in terms of $\hat{y}$ and $\hat{p}_y$ (equation (26)), and $Q(x)$ and $P(x)$ in terms of y_{u}, y_{s}, p_{u} and p_{s} (equation (18)), there results

$$\hat{H} - E_\gamma = \frac{\lambda\dot{x} f'}{J}\left[-y_{\mathrm{u}}y_{\mathrm{s}}\hat{p}_y^2 + (y_{\mathrm{u}}p_{\mathrm{s}} + p_{\mathrm{u}}y_{\mathrm{s}})\frac{\hat{y}\hat{p}_y + \hat{p}_y\hat{y}}{2} - p_{\mathrm{u}}p_{\mathrm{s}}\hat{y}^2\right] \tag{37}$$

in accordance with equation (33).

5. Resonances with minimum energy dispersion. The scar function

In the previous section we constructed a basis of resonances (associated with a given PO γ) at a particular Bohr–Sommerfeld-quantized energy E_γ. In this section we are going to evaluate functions with minimum dispersion in that basis, and we will call them scar functions. That is, a scar function ϕ_γ is a linear combination of resonances of γ (normalized to unity for convenience)

$$\phi_\gamma = \sum_{j=0}^{N} c_j\psi_\gamma^{(4j)} \Big/ \sqrt{\textstyle\sum_{j=0}^{N} c_j^2} \tag{38}$$

with minimum dispersion σ, where

$$\sigma^2 \equiv \langle\phi_\gamma|(\hat{H}-E_\gamma)^2|\phi_\gamma\rangle = \langle\phi_\gamma|\hat{H}_{\rm h}^2|\phi_\gamma\rangle \tag{39}$$

according to equation (33). The sum in equation (38) only includes terms four excitations away from each other as results from equation (36). N is the maximum number of terms given by equation (30) and criteria below. Replacing (38) in (39) and using equation (35) we have

$$\Gamma^2 \equiv \frac{\sigma^2}{\mathcal{E}^2} = \sum_{j=0}^{N}\left[c_j\sqrt{(4j+1)(4j+2)}+c_{j+1}\sqrt{(4j+3)(4j+4)}\right]^2 \Big/ \sum_{j=0}^{N} c_j^2 \tag{40}$$

with $\mathcal{E} = (\hbar\lambda/2)\sqrt{\langle(\dot{x}f')^2\rangle}$, and where $\langle\rangle$ indicates the time average over the orbit. From the last relation we see immediately that Γ is a universal function which only depends on N; that is, it is independent of the system and of the particular PO. We will call it the universal dispersion.

Using the well known method of Lagrange's undetermined multipliers, the minimum value of Γ is obtained from the following system of equations:

$$A_{j-1}c_{j-1} + (B_j - \Gamma^2)c_j + A_j\, c_{j+1} = 0 \tag{41}$$

for $j = 0, \ldots, N$, with

$$\begin{aligned} A_j &= \sqrt{(4j+1)(4j+2)(4j+3)(4j+4)} \\ B_j &= (4j-1)4j + (4j+1)(4j+2). \end{aligned} \tag{42}$$

Actually, this system of equations represents the following eigenvalue problem:

$$(\hat{H}_{\rm h}/\mathcal{E})^2\phi_\gamma = \Gamma^2\phi_\gamma \tag{43}$$

with

$$\begin{aligned} A_j &= \langle\psi_\gamma^{(4j)}|\hat{H}_{\rm h}^2/\mathcal{E}^2|\psi_\gamma^{(4j+4)}\rangle \\ B_j &= \langle\psi_\gamma^{(4j)}|\hat{H}_{\rm h}^2/\mathcal{E}^2|\psi_\gamma^{(4j)}\rangle. \end{aligned} \tag{44}$$

By replacing recursively the coefficients in (41) (putting c_N in terms of c_{N-1} and so on), we obtain an expression for Γ^2 in the continued-fraction form

$$\Gamma^2 = B_0 - \cfrac{A_0^2}{(B_1-\Gamma^2) - \cfrac{A_1^2}{(B_2-\Gamma^2) - \cdots - \cfrac{A_{N-1}^2}{(B_N-\Gamma^2)}}} \tag{45}$$

which can be solved self-consistently by setting $\Gamma = 0$ as the initial value on the left-hand side of equation (45). The convergence of this problem is exponential and the solution is reached in a few steps.

Now, taking $c_0 = 1$, there results $c_1 = -(B_0 - \Gamma^2)/A_0$ and the recursive relation

$$c_{j+1} = -\frac{A_{j-1}c_{j-1} + (B_j - \Gamma^2)c_j}{A_j} \tag{46}$$

for $j = 1, \ldots, N-1$. In this way we have obtained the fundamental scar function which consists of even transverse excitations. A similar construction can be done with odd excited resonances: $\psi^{(1)}, \psi^{(5)}, \psi^{(9)}, \ldots$. In this case the same relations are valid if we replace $4j$ by $4j+1$ in equations (38), (40), (42) and (44).

In order to obtain asymptotic expressions for Γ and the coefficients c_j as $N \to \infty$, we define a continuous function $c(z)$ in the range $0 < z \leqslant 1$, so that

$$c(z_j) = (-1)^j c_j \qquad \text{with} \quad z_j \equiv j/(N+1).$$

Then, the recursive relation (41) transforms into the following ordinary differential equation:

$$4z^2\frac{\mathrm{d}^2c(z)}{\mathrm{d}z^2}+8z\frac{\mathrm{d}c(z)}{\mathrm{d}z}+\left(1+\frac{\Gamma^2}{4}\right)c(z)=0 \tag{47}$$

restricted by the boundary condition $c(1)=0$ (because $c_{N+1}=0$). To obtain equation (47), we have expanded the roots in equation (42) by assuming $j\gg 1$, so the differential equation is a poor approximation to the recursive relation for $z=\mathcal{O}(1/N)$.

A positive well behaved solution of equation (47) is given by

$$c(z)=-\frac{\sin[(\Gamma/4)\ln z]}{\sqrt{z}}. \tag{48}$$

Actually, we have obtained numerically that an improved expression for the coefficients, which corrects the error of the first ones, is given by

$$c_j=(-1)^j(1-\beta/j)c(z_j) \tag{49}$$

with $\beta\simeq(0.132\pm 0.003)(1-1/N)/\ln^{1/4}(N+1)$ (this expression was verified in the range $1\leqslant N\leqslant 10^5$). The analysis shows that the error of equation (48) is very small and limited to the first coefficients.

Equation (48) provides the coefficients c_j for $j\geqslant 1$ (for simplicity, we do not use the improved expression of equation (49)). The value of c_0 is derived directly from (41) in terms of c_1; that is, $(1-\Gamma^2/2)c_0=-\sqrt{6}c_1$.

With the coefficients at hand, we evaluate the sums in equation (40); in terms of integrals for $j\geqslant 1$. Moreover, defining $u\equiv-(\Gamma/4)\ln z$, integrals are solved explicitly. For instance,

$$\frac{1}{N}\sum_{j=0}^{N}c_j^2\simeq\frac{6\sin^2(u_1)}{(1-\Gamma^2/2)^2}+\frac{2}{\Gamma}\left(u_1-\frac{\sin(2u_1)}{2}\right) \tag{50}$$

with $u_1=(\Gamma/4)\ln(N+1)$. Then, after some algebra equation (40) takes the following simple form:

$$\cot(u_1)=3\Gamma/(2-\Gamma^2). \tag{51}$$

From this equation there results an expression for $\Gamma(N)$. If $\Gamma\to 0$ for $N\to\infty$, the right-hand side of equation (51) goes to zero and then u_1 goes to $\pi/2$, so Γ goes to zero as $2\pi/\ln N$ in accordance with the starting assumption. This asymptotic behaviour is exact because the contribution of the first coefficients (which have a small error) in equation (40) goes to zero as $N\to\infty$. On the other hand, for $N=0$ it turns out that $u_1=0$ and from (51) we obtain $\Gamma^2=2$, which is the exact value. However, the evaluation of Γ for $N\geqslant 1$ is not wholly correct, although of course the error goes to zero for large values of N. To improve the solution for low values of N, we change the previous expression of u_1 by

$$u_1=(\Gamma/4)\ln(N/\alpha+1). \tag{52}$$

This new expression is justified because the $N=0$ case is guaranteed for any $\alpha>0$ and the asymptotic behaviour does not change. We can consider that α introduces an effective lower limit of integration, when the sums in equation (40) are approximated by integrals, in order to improve the approximation and to correct the error of the first coefficients. By taking $\alpha\simeq 1.35$, the $N=1$ case is corrected, and equation (51) gives good values of Γ for all N.

An explicit expression for Γ is obtained from equation (51) by writing u_1 in terms of Γ and expanding it around $\Gamma=0$. By taking only the first three terms of the asymptotic expansion, we obtain the following expression (valid for the fundamental or even scar function):

$$\Gamma(N)\simeq\frac{2\pi}{A-6\pi^2/A^2} \tag{53}$$

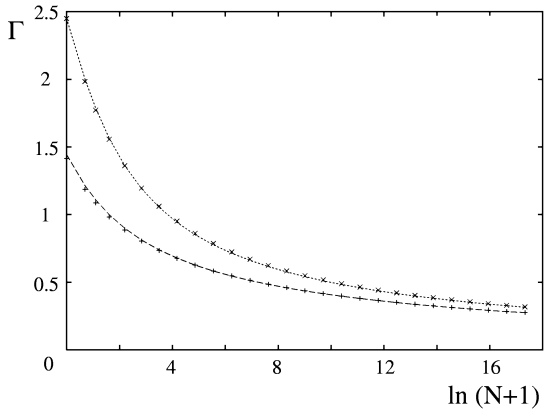

Figure 5. Plot of Γ against $\ln(N+1)$. Symbols ((+) for the even scar function and ($\times$) for the odd one) correspond to the exact coefficients numerically obtained with equation (45) and curves show the behaviour of expressions given in equations (53) and (54). The agreement is excellent.

with $A = 6 + \ln(N/1.35 + 1)$.

For odd scar functions, equations (47) and (48) are exactly the same, $(1 - \Gamma^2/6)c_0 = -\sqrt{10/3}c_1$ and $\cot(u_1) = 5\Gamma/(6 - \Gamma^2)$. The corresponding explicit expression is given by

$$\Gamma_{\text{odd}}(N) \simeq \frac{2\pi}{A' - (70\pi^2/3^4)/A'^2} \tag{54}$$

with $A' = 10/3 + \ln(N/1.95 + 1)$. $\Gamma^2 = 6$ for $N = 0$, and it goes to zero as $2\pi/\ln N$ for large N, adopting the same asymptotic behaviour as the even case. Figure 5 shows the excellent fit of the obtained solutions (equations (53) and (54)) with the exact numerical computation derived from equation (45).

The scar functions studied so far have zero mean transverse energy. They are related to the solutions given in [9] with zero energy. In order to obtain solutions with mean transverse energy $\beta\mathcal{E}$, it is necessary to solve the following eigenvalue problem:

$$(\hat{H}_{\text{h}}/\mathcal{E} - \beta)^2\phi_\gamma = \Gamma^2\phi_\gamma. \tag{55}$$

In this case, the excitations $\psi^{(2)}, \psi^{(6)}, \psi^{(10)}, \ldots$, ($\psi^{(3)}, \psi^{(7)}, \psi^{(11)}, \ldots$, for odd scar functions), with pure imaginary coefficients, are incorporated into ϕ_γ (equation (38)) in order to solve equation (55). Of course, the dispersion increases with respect to the $\beta = 0$ case. Explicit expressions will be given in [21].

6. Numerical results

6.1. The Bunimovich stadium billiard case

In this section we provide an application of this new construction to the Bunimovich stadium billiard, a classically chaotic system [22]. Taking the set of POs shown in figure 6, we have calculated its corresponding scar functions (the even and odd scars, always referenced as 'number of the orbit-0' and 'number of the orbit-1' correspondingly). They are displayed in both configuration and phase space (Husimi) representations in figures 7 and 8. Figure 7 shows that self-focal points influence the shape of these functions; scar functions diverge (in agreement with [6]) with $\hbar$ in these points. This is the main difference between scar functions and the resonances employed to construct them (for a comparison see figure 9). This feature

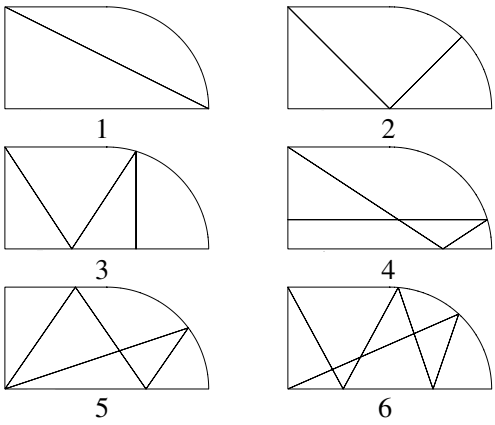

Figure 6. Orbits used in the present construction. Numbers appearing below each of them are used to label the corresponding scar functions.

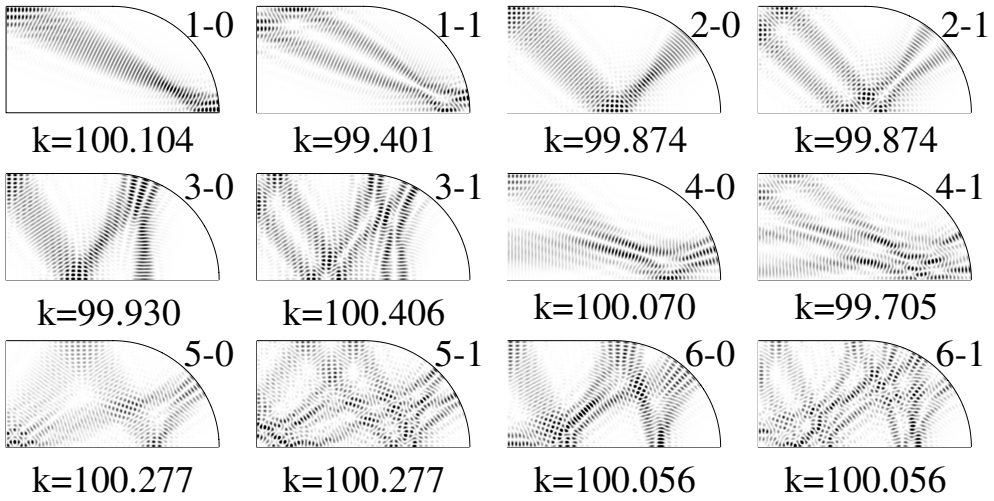

Figure 7. Linear density plots of scar functions in configuration space. Scar functions are labelled as indicated in the main text (0 for the even state and 1 for the odd one). Numbers appearing below are the Bohr–Sommerfeld values of the wavenumber.

can be better understood with the aid of the Husimi representation (figure 8). This behaviour is easily explained because now it can be clearly seen that the function sticks to the stable and unstable manifolds of each orbit. These latter are represented by the curves passing through the fixed points associated with the POs in our surface of section in Birkhoff coordinates. Dots indicate the locations of the zeros of the Husimi functions. We have chosen scar functions with their wavenumbers nearest to 100. In figure 9 we show the first four out of a total of five resonances needed to construct the scar function '2–0', i.e. the even scar corresponding to the orbit labelled 2. It is important to note that the vacuum state has already been constructed in [2] and that the explicit construction of its excitations for the case of the stadium will be reported in [21].

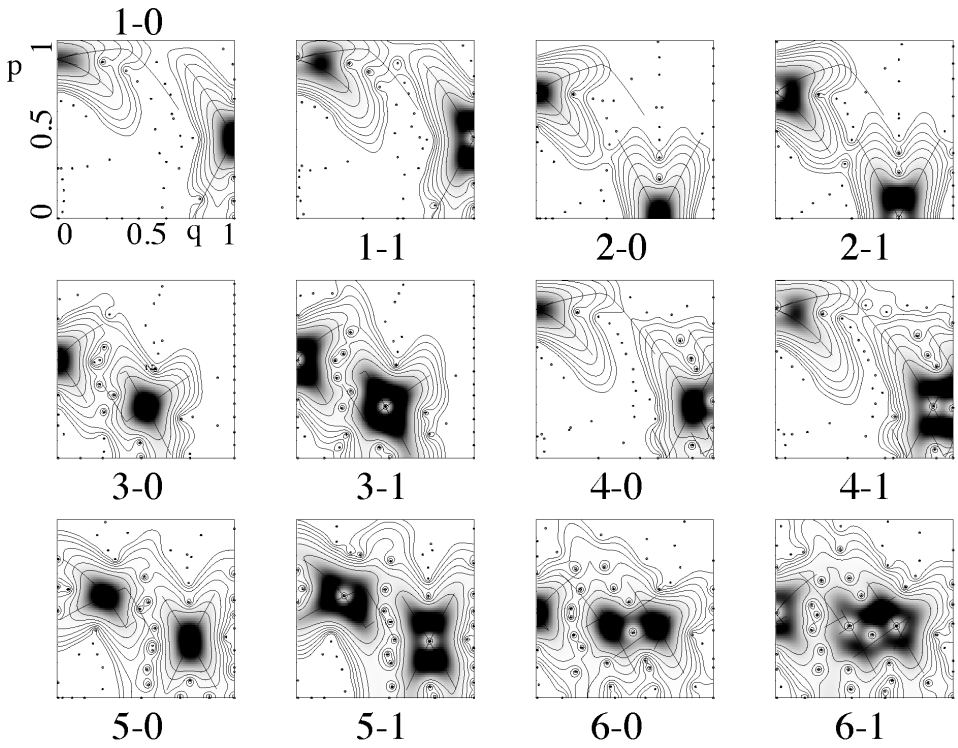

Figure 8. Linear density plots of Husimi distributions corresponding to the scar functions displayed in figure 7. A logarithmic scale of uniform level ratio $1/e$ from the maximum downwards was used in the contour plots. Different levels of grey, uniformly distributed, complete this picture. Dots are located at each zero of the Husimi functions. Solid curves passing through the fixed points represent the stable and unstable manifolds.

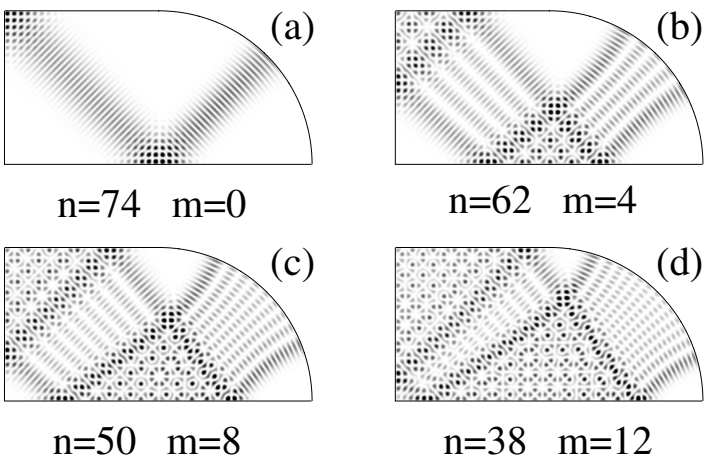

Figure 9. Linear density plot for four of the five resonances needed to construct the scar function 2–0. (*a*) $n = 74$, $m = 0$ (the vacuum state). (*b*) $n = 62$, $m = 4$ (first contributing excitation). (*c*) $n = 50$, $m = 8$. (*d*) $n = 38$, $m = 12$.

Table 1. Numerically calculated dispersion σ_γ versus the semiclassically predicted σ_k. The number of each scar function (coding explained in the main text) is displayed in the first column. The semiclassical and numerical values for the dispersion appear in the second and third columns; the ratios are displayed in the fourth one. The last column shows the sum of the squared overlap coefficients used in the calculation.

Scar function	σ_k	σ_γ	σ_k/σ_γ	$\Sigma_i \lvert d_i\rvert^2$
1–0	0.213	0.206	1.03	0.994
1–1	0.332	0.325	1.02	0.981
2–0	0.193	0.184	1.05	0.998
2–1	0.311	0.292	1.07	0.995
3–0	0.187	0.179	1.04	0.987
3–1	0.294	0.266	1.10	0.986
4–0	0.201	0.206	0.98	0.996
4–1	0.311	0.295	1.05	0.991
5–0	0.191	0.185	1.03	0.994
5–1	0.298	0.298	1.00	0.983
6–0	0.197	0.190	1.04	0.987
6–1	0.309	0.290	1.07	0.982

One of the most important properties of scar functions, to test the semiclassical expressions, is the dispersion. In order to evaluate numerically the dispersion of scar functions, we have calculated the overlaps of their normal derivatives (over the boundary of the stadium) with the exact eigenfunctions. We have taken a known norm [23] for normal derivatives over the boundary, which gives the expression for the overlap $\langle\psi_1|\psi_2\rangle = \int \partial_n\psi_1\partial_n\psi_2(r_n/2k^2)\,\mathrm{d}s$, where $r_n = \vec{r}.\hat{n}$ with $\hat{n}$ the outgoing unit normal vector and s the arclength. The evaluation of the overlaps has been performed inside a window of the spectrum centred at the Bohr–Sommerfeld wavenumber k_{BS} for the corresponding scar function. Then, the dispersion in the k-spectrum is $\sigma_\gamma^2 = \sum_i |d_i|^2(k_i - k_{\mathrm{BS}})^2$, where k_i is the eigen-wavenumber of the eigenfunction ψ_i, and $d_i = \langle\phi_\gamma|\psi_i\rangle$. Table 1 shows the semiclassically predicted value $\sigma_k = \sigma_{k^2}/(2k) = \Gamma(N)\lambda/2$ for the scar functions in the second column. The third column shows the corresponding values of the numerically calculated dispersion σ_γ. Finally, the fourth one displays the ratios σ_γ/σ_k. It is clear that the overwhelming majority of them is highly accurate. In figure 10 we show the plots of the Gaussian smoothed curves made from the squared overlap coefficients. The smoothing was done by including a Gaussian factor in each d_i value. The final curve is the sum

$$f_{\mathrm{sm}}(k) = \Delta \sum_i |d_i|^2\ \mathrm{e}^{-(k-k_i)^2/(2\sigma^2)} \Big/ \sqrt{2\pi\sigma^2}$$

where $\Delta = 1/\rho_k = 2\pi/(Ak)$ is the mean level spacing, A being the area of the billiard and ρ_k the mean level density. In performing the smoothing, dispersion σ was taken such that $\sigma^2 = \sigma_\gamma^2/10$, which is an intermediate value in the sense that while avoiding fine structures that could hide the general (well predicted) behaviour it reveals the underlying complexity. In fact, many interesting phenomena can be investigated with the aid of finer structure scales and we are working in that direction at the moment. To conclude, these curves can be directly compared with the also plotted theoretical Gaussian curves

$$f_{\mathrm{th}}(k) = \Delta \exp\left[-(k - k_{\mathrm{BS}})^2/(2\sigma_k^2)\right] \Big/ \sqrt{2\pi\sigma_k^2}.$$

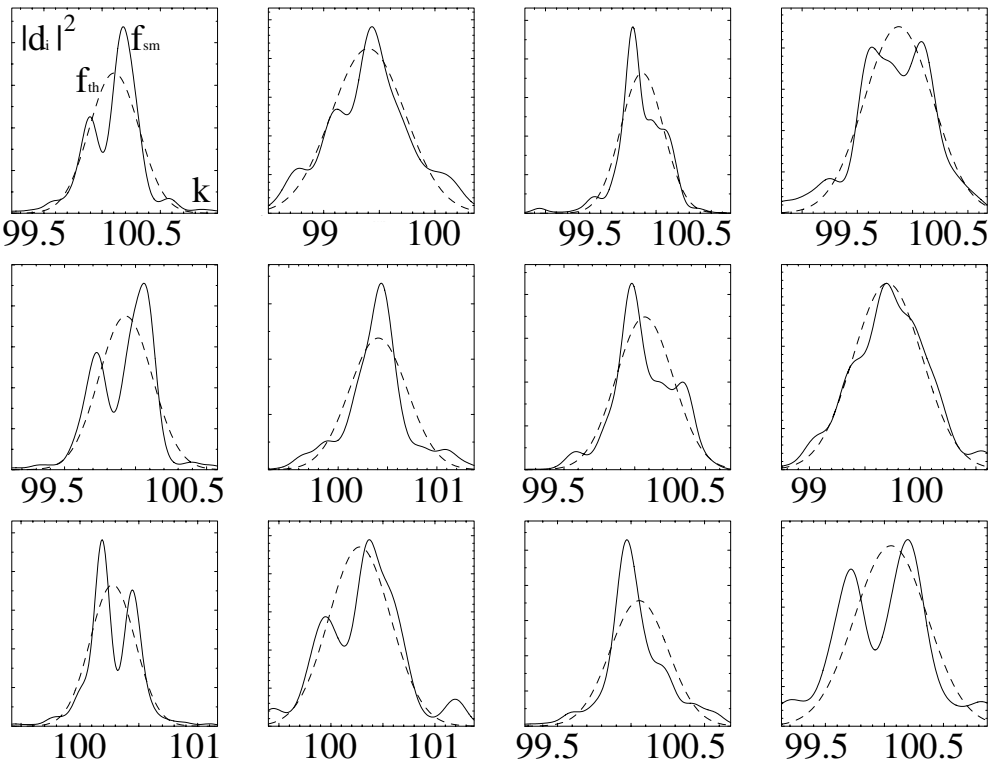

Figure 10. Solid curves correspond to the smoothed squared overlaps of each scar function with the exact eigenfunctions ($f_{\rm sm}$) versus wavenumber k. Dashed curves represent the theoretical Gaussians $f_{\rm th}$.

6.2. Study of the transverse component of the scar function

In this part we will proceed with the numerical analysis of scar functions restricted to a given transverse section, that is for a fixed value of x. We will consider the situation where $\xi_{\rm u} = \hat{e}_y$ and $\xi_{\rm s} = \hat{e}_{p_y}$, in order to compare with the results of [9]. This implies that $y_{\rm u} = 1$, $p_{\rm u} = 0$, $y_{\rm s} = 0$ and $p_{\rm s} = 1$ (see equations (9) and (10)). With them, there results from equation (14) the Hamiltonian (setting $\lambda \dot{x} f'/J = 1$) $H_{\rm h} = y p_y$, and its quantization $\hat{H}_{\rm h} = (\hat{y}\hat{p}_y + \hat{p}_y\hat{y})/2$ from equation (37).

The curves of constant energy, with $E > 0$ or $E < 0$, are hyperbolas in phase space ($p_y = E/y$). For $E = 0$, the motion occurs on the manifolds. There are two eigenfunctions for each value of the energy, one of them symmetric and the other antisymmetric with respect to the origin $y = 0$. The general expression for $y > 0$ is $\exp(\mathrm{i}E \ln y)/\sqrt{y}$ [24] (taking $\hbar = 1$), and we stress that the semiclassical prescription of equation (16) gives the same result, where $S = E \ln y$ and $\dot{y} = y$. These solutions are not square integrable; i.e. they cannot be normalized.

For our construction we have $Q = 1$ and $P = \mathrm{i}$. Later, equation (28) reduces (up to a global phase independent of m) to the eigenfunctions of the one-dimensional harmonic oscillator

$$\psi^{(m)}(y) = \frac{e^{-\mathrm{i}m\pi/4}}{\sqrt{2^m m!}} H_m(y) \frac{e^{-y^2/2}}{\pi^{1/4}}. \tag{56}$$

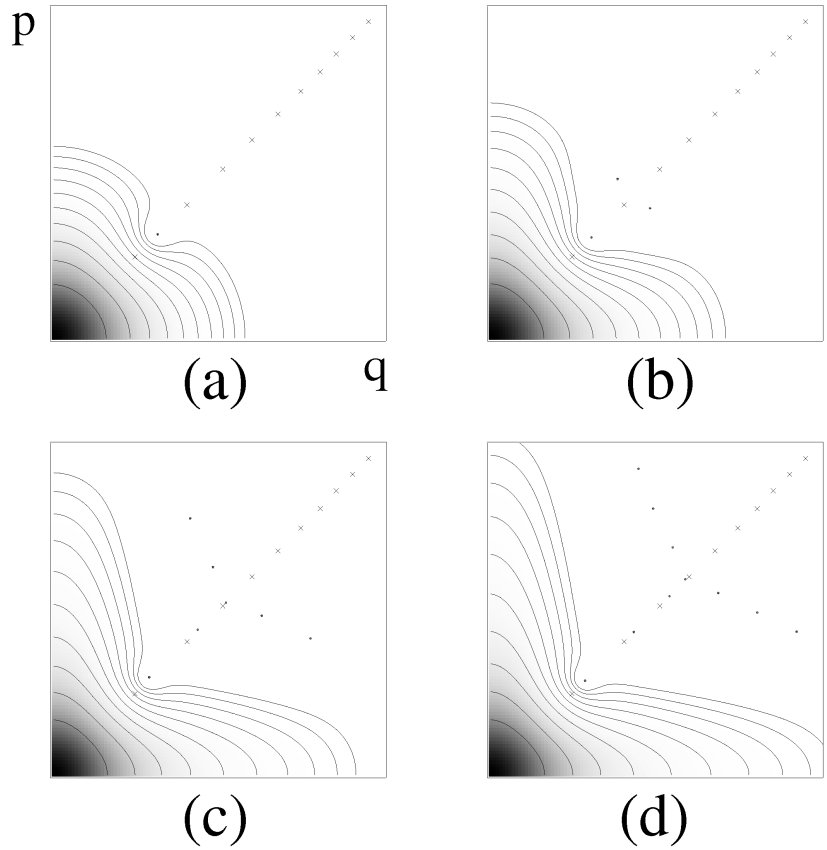

Figure 11. Husimi plots of the fundamental or even scar functions constructed for the Hamiltonian $H = yp_y$. We use the same scales of figure 8 for the contour plots and the levels of grey. (*a*) Here the number of excited terms in the series is $N = 1$. (*b*) $N = 3$. (*c*) $N = 7$. (*d*) $N = 10$. The dots correspond to their zeros while the crosses are placed at the zeros of the symmetric eigenfunction.

The greater the number of excitations included, the better the approximation to the corresponding eigenfunction, but we must remember that in the context of our construction this number is limited by the transverse area A_{lin} of phase space where the linearization is valid (see section 4). In figure 11 we can see the Husimi plots for the even scar functions associated with this Hamiltonian. The same logarithmic scale as previously used in the Bunimovichh stadium example has been taken for the contour lines, supplemented by a linear density plot. Both of them show that the maximum intensity of the functions lies along the stable and unstable manifolds (the vertical and horizontal axes respectively) associated with the hyperbolic fixed point at the origin. We have selected some examples of scar functions constructed with a number of terms $N = 1, 3, 7$ and 10 (resonances) in the corresponding sums. The number of their zeros (denoted by dots) is equal to four times this value (it is useful to have in mind that we are showing only a quarter of the full phase space; the remaining parts of this picture can be easily obtained by reflecting with respect to the horizontal and vertical axes). This is so due to the fact that the Hermite polynomials involved in these expressions have a maximum order equal to $4N$, this being the number m of transverse excitations of the resonances. On the other hand, we have also plotted the zeros of the symmetric eigenfunction with $E = 0$ (these zeros

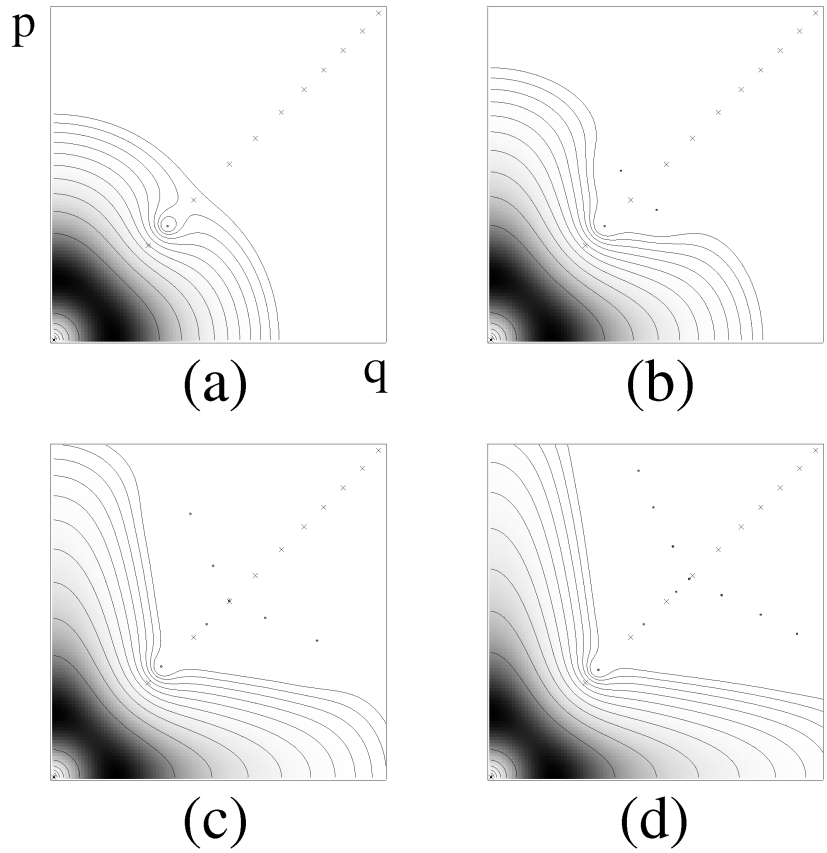

Figure 12. Husimi plots of the odd scar functions constructed for the Hamiltonian $H = yp_y$. We use the same scales as in the previous figure. (*a*) $N = 1$. (*b*) $N = 3$. (*c*) $N = 7$. (*d*) $N = 10$. The dots correspond to their zeros while the crosses are placed at the zeros of the antisymmetric eigenfunction.

were investigated in [9]). It can be seen that the zeros of each scar function are close to those corresponding to the exact ones in the relevant region, whilst they differ in the region where the functions are exponentially small. Moreover, as the number of the terms included in the sum grows, the number of coincident zeros and their accuracy also increases. Nevertheless, in the exponentially small region, they go away from the cuve where all the exact ones lie, doing this symmetrically with respect to this curve in a 'V'-shaped form (the number of zeros also grows on this 'V'). We want to underline the great similarity between the even scar functions and the symmetric eigenfunction because the positions of the zeros of these functions are a very sensitive measure of any difference or perturbation. Moreover, in figure 12 we show the same type of plot but for the odd scar functions together with the zeros of the antisymmetric eigenfunction. In this case, the description is similar to the even case but with the inclusion of a zero at the origin.

Finally we want to note that the solutions for any other configuration of the unstable and stable manifolds (as could happen for different points along a periodic trajectory) will behave in the same way as in the previously discussed example. The only important point to underline is that the manifolds will change their position accordingly with a symplectic transformation, and

the new transverse functions will be a metaplectic transformation [13] of the functions shown before. In order to clarify this idea we can take another simple case where ξ_u and ξ_s are now rotated by $\pi/4$ in the anticlockwise sense with respect to the previous case. This implies that $\xi_u = (\hat{e}_y + \hat{e}_{p_y})/\sqrt{2}$ and $\xi_s = (-\hat{e}_y + \hat{e}_{p_y})/\sqrt{2}$. Replacing these new values in the hyperbolic Hamiltonian we obtain $H_h = (p_y^2 - y^2)/2$ from equation (14) and its quantization $\hat{H}_h = (\hat{p}_y^2 - \hat{y}^2)/2$ from equation (37). In this case $Q = (1-i)/\sqrt{2}$ and $P = (1+i)/\sqrt{2}$. Then, we must add the factor $\exp[im\pi/4]$ to the transverse component of the excitations written in equation (56).

7. Conclusions and final remarks

The use of scar functions instead of vacuum states in the theory of short POs introduces strong conceptual and practical differences. From the theoretical point of view, notice in the first place that the overlap between a scar function and its related vacuum state goes logarithmically to zero with $\hbar$. This is derived directly from equation (50). The square of the overlap is given by the first right-hand side term (which represents c_0^2/N) divided by $\frac{1}{N}\sum_{j=0}^{N} c_j^2$. In this respect, scar functions acquire a wholly different character as $\hbar$ goes to zero. They are not simply a sophisticated version of vacuum states, but they mimic the classical structure which organizes the short-time dynamics, and then we hope phase space will be covered more efficiently and uniformly.

Of course, it is possible to justify quantitatively the use of scar functions. In section 5 we have proved that the universal dispersion Γ goes to zero with $\hbar$ (again logarithmically). So, scar functions are much more localized in energy than vacuum states. In fact, they converge formally on each transverse plane (to the orbit), to the eigenfunctions of the quadratic Hamiltonian derived from the return map (the eigenfunctions investigated in [9]). Notice that they are not eigenfunctions of the system. We can illustrate this point as follows. If $\sigma\rho$ goes to zero, the wavefunction goes to an eigenfunction, but σ behaves like $\hbar/|\ln\hbar|$, $\rho = \mathcal{O}(\hbar^{-1})$ for the transverse direction (one degree of freedom) and $\rho = \mathcal{O}(\hbar^{-2})$ for the system.

Another justification (perhaps the same) for the use of scar functions is that they acquire in the semiclassical limit the hyperbolic structure characteristic of unstable orbits. The work of Percival [25] teaches us that classical phase space structures dominate the semiclassical behaviour. Following the same philosophy, we claim that in the semiclassical limit the unique proper basis of wavefunctions to obtain chaotic eigenfunctions is the basis of scar functions (constructed with the shortest POs of the system [1]).

In the second place, notice that matrix elements between scar functions around different POs go to zero at most as a power of $\hbar$ (using vacuum states they decrease exponentially with $\hbar$ [1]). We are thinking about smooth operators which do not destroy the hyperbolic structure, for instance the Hamiltonian operator. The application of the Hamiltonian to a scar function has a Husimi distribution similar to that observed in figure 8 but with two (three) zeros at each fixed point for the even (odd) case. Then, the overlap does not decrease exponentially because the two hyperbolic structures (related to the considered POs) are always in contact; on a Poincaré surface of section the intersection points are so-called heteroclinic.

On the practical level, we have learned that the contribution of POs to eigenfunctions is not restricted to the vacuum contribution. For example, in figure 13(*a*) we show a highly excited eigenfunction of the stadium billiard. This state is the linear combination of around 1000 plane waves; so, the contribution of each plane wave is around 0.1%. The state has a scar of orbit two (see figure 6). The vacuum contribution of this orbit (see figure 13(*b*)) reproduces 6.2% of the state, while the corresponding scar function (see figure 13(*c*)) 8.6%. Moreover, figure 13(*a*) shows clearly the self-focal point appearing in the scar function.

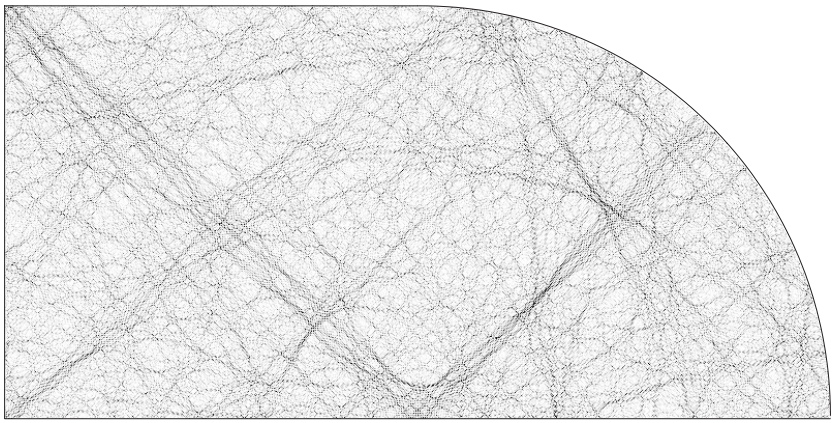

(*a*)

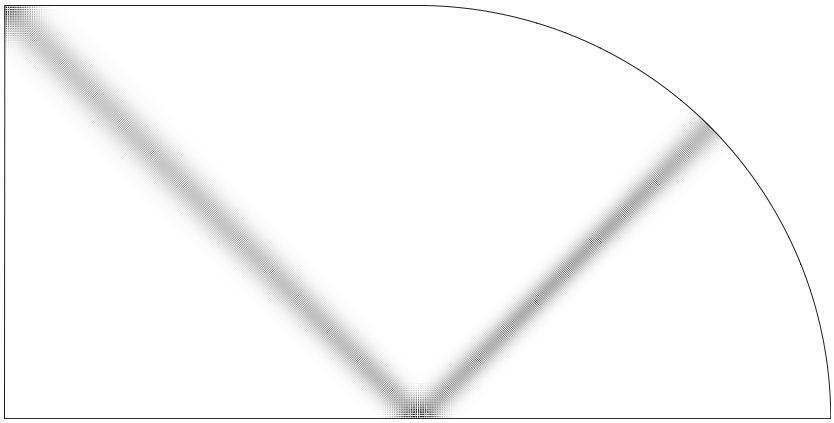

(*b*)

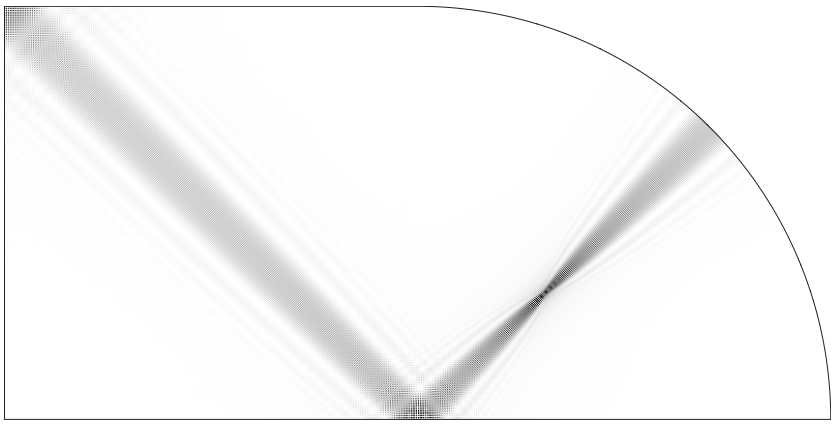

(*c*)

Figure 13. Linear density plot of: (*a*) the odd–odd eigenfunction at $k = 1000.41648$ for the stadium billiard; (*b*) the vacuum state of orbit two and (*c*) the scar function of orbit two.

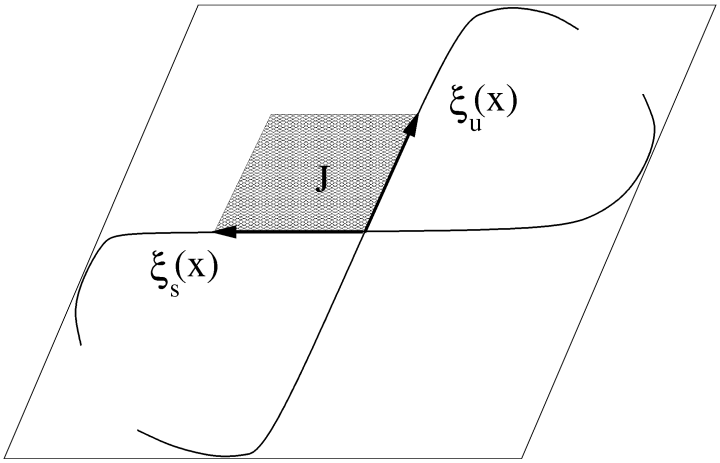

Figure 14. Parallelogram with symplectic area corresponding to the definition given in remark (*i*), i.e. an upper limit of the area where the linear regime works. The inner parallelogram of unit area (J) defined by the stable and unstable directions is similar to the exterior one.

Finally, we want to point out some remarks and ideas that are relevant for further extensions and applications of the construction developed throughout this paper:

(i) The decomposition of the motion in the vicinity of a PO, into a periodic and a hyperbolic one, depends on the function $f(x)$ (see section 2). This function, that determines the dilation–contraction rate along the manifolds, was only defined at $x = 0$ and $x = L$ ($f(0) = 0$ and $f(L) = L$). A reasonable way of imposing further conditions on f is by requiring that the projections of $\xi_u(x_i) = \xi_s(x_i)$ on each axis are equal in absolute value at all the points x_i. At these points the manifolds are symmetrical with respect to the axes y and p_y (see section 2). These conditions are based on the fact that position and momentum have different physical meaning. For this reason they do not resist symplectic transformations of the transverse axes y and p_y. Nevertheless, once the function f is defined, the constructed resonances are invariant with respect to symplectic transformations of the transverse variables.
The motion can be decomposed in a symplectic invariant fashion if we have information on the nonlinear regime in the vicinity of the PO. Figure 14 shows a transverse section at a given value of x, where the manifolds in the nonlinear regime are included. Drawing straight lines tangential to one of the manifolds and parallel to the linear direction of the other, a parallelogram is defined. Then, it is possible to select $\xi_u(x)$ and $\xi_s(x)$ such that these vectors define a parallelogram (with unit area) similar to the previous one. Having these vectors for all values of x, $F(x)$ is automatically defined in a symplectic invariant way.
On the other hand, the area of the defined parallelogram is an upper limit of the area where the linear regime works, and we expect that this area goes to zero exponentially with the period of the orbit. In such a case, scar functions of short POs will have the smallest universal dispersion. This is a quantitative justification of the central role played by the shortest POs in the theory of short POs.

(ii) Using heuristic arguments, Kaplan and Heller [12] have proposed a semiclassical construction of localized wavefunctions on fixed points in maps. These functions are similar to the even scar functions (restricted to a section) presented in this article. Moreover, their approach can be extended to fluxes by using the decomposition of the transverse motion

explained in section 2. However, we stress that our construction has the advantage of providing explicit expressions.

(iii) The scar functions are eigenfunctions of $\hat{H}_{\parallel} + \hat{H}_{\mathrm{p}}$ which minimize the dispersion of $\hat{H}_{\mathrm{h}}$. On the other hand, the semiclassical theory of short POs [1, 2] gives a recipe to obtain eigenfunctions of $\hat{H}_{\parallel} + \hat{H}_{\mathrm{p}} + \hat{H}_{\mathrm{h}}$ as a linear combination of scar functions of short POs. If $H_{\parallel} + H_{\mathrm{p}} + H_{\mathrm{h}}$ were a quadratic approximation of H (see equation (15)) in the vicinity of each short PO, the error of the obtained semiclassical eigenfunctions would be $\mathcal{O}(\hbar)$, as discussed after equations (20) and (33). However, $H_{\parallel} + H_{\mathrm{p}} + H_{\mathrm{h}}$ is a synchronized motion approximation of H (it is quadratic in the transverse direction), and then the semiclassical eigenfunctions have an error $\mathcal{O}(\sqrt{\hbar})$ as explained in appendix A.

(iv) The universal dispersion $\Gamma(N)$ decays very slowly in the extreme semiclassical limit (the behaviour $1/\ln N$ was predicted in [12] using simple arguments). From reviewing a great number of exact eigenfunctions of the Stadium billiard, we observed that odd scar functions are not as relevant as even ones. This fact can be understood by looking at figure 5, where the odd universal dispersion is greater than the even one, and they are comparable only for very large values of N.

(v) Recently, based on trace formulas, Wisniacki and Vergini [26] have constructed smooth functions highly localized in the neighbourhood of POs using only quantum information. They are obtained by Fourier transforming the probability density of eigenfunctions. These smooth functions show an impressive similarity with a combination of the even and odd scar functions constructed in this article. We can say that they are a coherent contribution of even and odd scar functions when μ is an even number; that is, when the linearized motion is hyperbolic without reflection. In this case, even and odd scar functions quantize at the same energies. When the motion is hyperbolic with reflection (μ is an odd number), odd scar functions quantize at the anti-Bohr energies of the even case, and then even and odd scar functions contribute with opposite sign.

(vi) This new construction provides a precise definition of a scar function and will be very useful for quantifying scarring of individual states and studying scar phenomena in general. This a subject that has received much attention in the last years [27]. For instance, by reducing the degree of smoothing used to construct figure 10, many substructures appear, having much information regarding the interaction of these classically motivated objects.

Acknowledgments

This work was partially supported by PICT97 03-00050-01015 and SECYT-ECOS. We are really grateful to a referee for very helpful comments about the first version of this article.

Appendix A

In this appendix we consider a Hamiltonian of the form kinetic plus potential energy with the configuration space being the Euclidean plane. Then by taking the solution provided in section 3, which lives in the vicinity of the orbit γ, as the eigenfunction of the corresponding quantum Hamiltonian, we will be able to determine that the error involved in the semiclassical approximation is of order $\sqrt{\hbar}$. In section 3 we obtained an error of order $\hbar$ after neglecting some terms of the Hamiltonian in order to have a synchronized motion in the neighbourhood of the orbit.

We use the curvilinear coordinate system defined in section 2. A point in the vicinity of the orbit (in configuration space) is given by $\vec{r} = \vec{M}(x) + y\hat{e}_y$, where $\vec{M}(x)$ describes the curve

depicted by the orbit itself and $y\hat{e}_y$ a transverse displacement from it. Then the velocity is $\dot{\vec{r}} = \dot{x}\hat{e}_x + \dot{y}\hat{e}_y + \dot{x}y\hat{e}_x/\rho(x)$, where $\rho(x)$ is the radius of curvature of the trajectory at x. Later, the Lagrangian is $L = m(\dot{x}^2g^2 + \dot{y}^2)/2 - V(x, y)$, with $g = 1 + y/\rho(x)$, and the Hamiltonian in curvilinear coordinates takes the form

$$H = \frac{1}{2m}(p_x^2/g^2 + p_y^2) + V(x, y)$$

where $p_x \equiv mg^2\dot{x}(x, y)$ and $p_y \equiv m\dot{y}$.

For this Hamiltonian, $p_x = m\dot{x}$ and $p_y = m\dot{y} = 0$ on γ. Then, it turns out that

$$0 = -\dot{p}_y = -\frac{p_x^2}{m\rho} + \frac{\partial V}{\partial y}(x, 0) \tag{A.1}$$

on γ. Moreover, equation (1) takes the form

$$-\dot{p}_y = \left(3\frac{p_x^2}{m\rho^2} + \frac{\partial^2 V}{\partial y^2}(x, 0)\right) y. \tag{A.2}$$

The quantum Hamiltonian in curvilinear coordinates is [17]

$$\hat{H} = -\frac{\hbar^2}{2mg}\left(\frac{\partial}{\partial x}\frac{1}{g}\frac{\partial}{\partial x} + \frac{\partial}{\partial y}g\frac{\partial}{\partial y}\right) + V(x, y)$$

and we are going to show that

$$(\hat{H} - E)\psi(x, y) = \mathcal{O}(\hbar^{3/2}) \tag{A.3}$$

where

$$\psi(x, y) = \mathrm{e}^{(\mathrm{i}/\hbar)[S(x)+y^2P(x)/2Q(x)]}/\sqrt{p_x(x)Q(x)}.$$

Taking into account that $y = \mathcal{O}(\sqrt{\hbar})$, we can isolate each order in $\hbar$ of equation (A.3) as follows:

$$\hbar^0 : \frac{p_x^2}{2m} + V(x, 0) - E = 0$$

$$\hbar^{1/2} : y\left(-\frac{p_x^2}{m\rho} + \frac{\partial V}{\partial y}(x, 0)\right) = 0$$

$$\hbar^1 : \frac{y^2}{2}\left(\frac{3p_x^2}{m\rho^2} + \frac{\partial^2 V}{\partial y^2}(x, 0) + \frac{\dot{x}P'}{Q}\right) + (y^2P/Q - \mathrm{i}\hbar)(P/m - \dot{x}Q')/2Q = 0.$$

The $\hbar^0$ order is zero if $E = E_\gamma$. The next order, $\hbar^{1/2}$, is zero due to equation (A.1). Using that $\dot{x}Q' = \dot{Q}$ and $P/m = \dot{Q}$, the last term of $\hbar^1$ is zero. Moreover, the parenthesis of the first term is zero because $\dot{x}P' = \dot{P}$ and $\dot{P}/Q = -3p_x^2/m\rho^2 - \partial^2 V/\partial y^2(x, 0)$ according to equation (A.2).

In order to eliminate the term $\hbar^{3/2}$ of equation (A.3), it is necessary to include corrections of order $\sqrt{\hbar}$ in the solution.

Appendix B

The purpose of this appendix is to give a demonstration of equation (28). We can accomplish this by means of an inductive process. The case $m = 0$ is trivial. Using the definition (27) and equation (28), we have

$$\psi^{(m+1)} = \frac{\Lambda^\dagger}{\sqrt{(m+1)}}\frac{\mathrm{e}^{-\mathrm{i}m\phi}}{\sqrt{2^m m!}}H_m(\xi)\psi^{(0)}$$

where $\xi = y\sqrt{J/\hbar}/|Q|$. Then, equation (28) is valid for the case $m+1$ if and only if

$$H_{m+1}(\xi)\psi^{(0)} = \sqrt{2}\mathrm{e}^{\mathrm{i}\phi}\Lambda^{\dagger}H_m(\xi)\psi^{(0)}.$$

After applying $\Lambda^{\dagger}$ and taking into account that $\mathrm{e}^{\mathrm{i}(\phi+\eta)} = Q(x)/|Q(x)|$, it turns out that

$$H_{m+1}(\xi) = 2\xi H_m(\xi) - H'_m(\xi)$$

which is valid for Hermite polynomials [20].

References

[1] Vergini E G 2000 *J. Phys. A: Math. Gen.* **33** 4709
[2] Vergini E G and Carlo G G 2000 *J. Phys. A: Math. Gen.* **33** 4717
[3] Gutzwiller M C 1971 *J. Math. Phys.* **12** 343
[4] Berry M V and Keating J P 1990 *J. Physique* **23** 4839
Berry M V and Keating J P 1992 *Proc. R. Soc.* A **437** 151
[5] Voros A 1988 *J. Phys. A: Math. Gen.* **21** 685
[6] Bogomolny E B 1988 *Physica* D **31** 169
[7] Heller E J 1984 *Phys. Rev. Lett.* **53** 1515
[8] Berry M V 1989 *Proc. R. Soc.* A **423** 219
[9] Nonnenmacher S and Voros A 1997 *J. Phys. A: Math. Gen.* **30** 295
[10] de Polavieja G G, Borondo F and Benito R M 1994 *Phys. Rev. Lett.* **73** 1613
[11] Vergini E and Wisniacki D 1998 *Phys. Rev.* E **58** R5225
[12] Kaplan L and Heller E J 1999 *Phys. Rev.* E **59** 6609
[13] Littlejohn R G 1986 *Phys. Rep.* **138** 193
[14] Littlejohn R G 1988 *Phys. Rev. Lett.* **61** 2159
[15] Yakubovich V A and Starzhinskii V M 1975 *Lineal Differential Equations with Periodic Coefficients* (New York: Wiley)
[16] Heller E J 1991 *Proc. Les Houches Summer School on Chaos and Quantum Physics Les Houches Session LII* ed M J Giannoni, A Voros and J Zinn-Justin (Amsterdam: Elsevier)
[17] Babič V M and Buldyrev V S 1991 *Short-Wavelength Diffraction Theory* (Berlin: Springer)
[18] Eckhardt B and Wintgen D 1991 *J. Phys. A: Math. Gen.* **24** 4335
[19] Creagh S C, Robbins J M and Littlejohn R G 1990 *Phys. Rev.* A 1907
[20] Courant R and Hilbert D 1966 *Methods of Mathematical Physics* (New York: Interscience)
[21] Carlo G and Vergini E 2001 in preparation
[22] Bunimovich L A 1979 *Commun. Math. Phys.* **65** 295
[23] Vergini E and Saraceno M 1995 *Phys. Rev.* E **52** 2204
[24] Colin de Verdière Y and Parisse B 1994 *Commun. Part. Diff. Eqns* **19** 1535
[25] Percival I C 1973 *J. Phys. B: At. Mol. Phys.* **6** L229
[26] Wisniacki D A and Vergini E 2000 *Phys. Rev.* E **62** R4513
[27] Agam O and Fishman S 1994 *Phys. Rev. Lett.* **73** 806
Feingold M 1994 *Z. Phys.* B **95** 121
Simonotti F P, Vergini E and Saraceno M 1997 *Phys. Rev.* E **56** 3859
Arranz F J, Borondo F and Benito R M 1998 *Phys. Rev. Lett.* **80** 944
Kaplan L and Heller E J 1998 *Ann. Phys., NY* **264** 171
Toscano F, de Aguiar M A M and Ozorio de Almeida A M 2001 *Phys. Rev. Lett.* **86** 59